

pubs.acs.org/estengg Review

Outlook on Single Atom Catalysts for Persulfate-Based Advanced Oxidation

Xuanhao Wu and Jae-Hong Kim*



Cite This: ACS EST Engg. 2022, 2, 1776-1796



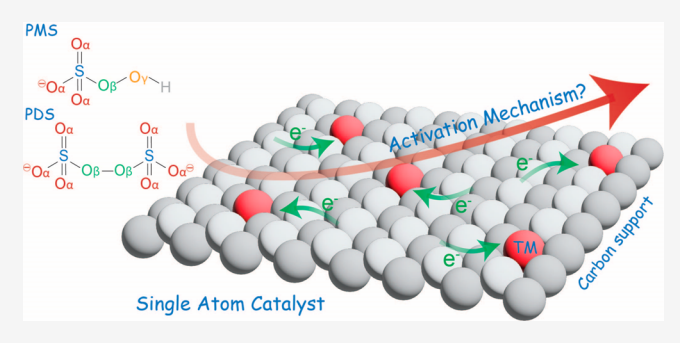
ACCESS I

Metrics & More

Article Recommendations

Supporting Information

ABSTRACT: Single atom catalysts (SACs) have emerged as a promising catalyst material architecture for energy, chemical, and environmental applications. In the past several years, SACs have been increasingly explored for persulfate-based advanced oxidation processes (AOPs) due to their superior persulfate activation and pollutant degradation performance compared to benchmark dissolved ion and nanoparticle catalysts. However, there still exist uncertainties on the mechanism of persulfate activation by SACs, which involves a complex interplay of sulfate and hydroxyl radicals, singlet oxygen, high-valent metal species, and/or mediated electron transfer. Questions also remain as to how persulfate ions



molecularly align on the single atom site, how persulfate ions are converted into reactive species, and what design parameters lead to higher efficiency for persulfate activation and pollutant degradation. In this critical review, we examine past SAC materials employed for persulfate-based AOPs and discuss how they function differently compared to their ion and nanoparticle counterparts. We further our discussion on current limitations, opportunities, and future research needs in (i) filling the knowledge gaps in the mechanisms of persulfate-SAC interactions; (ii) augmenting fundamental research with theoretical simulation and *in situ* characterization techniques; (iii) improving material design tailored for environmental applications; and (iv) proactively considering the challenges associated with engineering practices and complex water matrixes.

KEYWORDS: Single atom catalysts, advanced oxidation process, water treatment, persulfate, peroxymonosulfate

■ INTRODUCTION

Since the first introduction in 1987, advanced oxidation processes (AOPs) have been extensively studied and widely adopted to oxidatively destroy non-biodegradable and recalcitrant organic pollutants that are not effectively removed by conventional water treatment processes. To date, various AOPs have been developed, including Fenton, photocatalytic, and electrocatalytic systems.² Several precursor chemicals have been applied, including hydrogen peroxide (H2O2),3,4 persulfates such as peroxymonosulfate (PMS, HSO₅⁻) and peroxydisulfate (PDS, $S_2O_8^{2-}$), sulfite (SO_3^{2-}), and chlorine ($Cl_2/HOCl$). Among these, persulfate-based AOPs have been increasingly considered as a viable alternative to conventional H₂O₂-based AOPs due to their advantages, including longer half-life (30-40 μ s) and higher oxidation potential ($E^0(SO_4^{\bullet-}/SO_4^{2-}) = +2.60 \sim$ +3.10 V_{NHE}) of sulfate radicals (SO₄•-) than hydroxyl radicals (*OH, half-life = 1-100 ns, 9,10 E^{0} (*OH/OH $^{-}$) = $+1.90 \sim +2.70$ V_{NHE}), 11,12 high radical formation yield, 13 less dependence on pH, ^{14,15} and lower cost for storage and transportation of persulfate salt than H₂O₂ solution. To date, persulfate-based AOPs have been explored to oxidatively remove a wide range of organic pollutants such as polychlorinated biphenyls (PCBs), 16 polycyclic aromatic hydrocarbons (PAHs),¹⁷ petroleum hydrocarbons, 18 antibiotics, 19 pesticides, 20 phthalates, 21 and pharmaceuticals and personal care products (PPCPs) in various water remediation scenarios. 22

To activate persulfate and *in situ* produce reactive radicals such as SO₄• and •OH, both metal ions (homogeneous AOP) and metal nanoparticles (heterogeneous AOP) have been typically used as catalysts. For homogeneous catalysis, metals are applied either as ions (*e.g.*, Fe²⁺/Fe³⁺, ²³ Co²⁺/Co³⁺, ²⁴ Cu⁺/Cu^{2+2.5}) or complexed with chelating organics such as citric acid and ethylenediaminetetraacetic acid (EDTA) to form organometallic complexes (Figure 1a). ²⁶ The efficient contact between soluble catalysts with persulfate as well as between reactive radicals and target pollutants under mixing accounts for generally higher kinetics in homogeneous catalysis than heterogeneous catalysis. The main disadvantage of homogeneous catalysis is the difficulty of collecting and recycling soluble catalysts after use.

Received: May 25, 2022
Revised: August 19, 2022
Accepted: August 22, 2022
Published: September 7, 2022





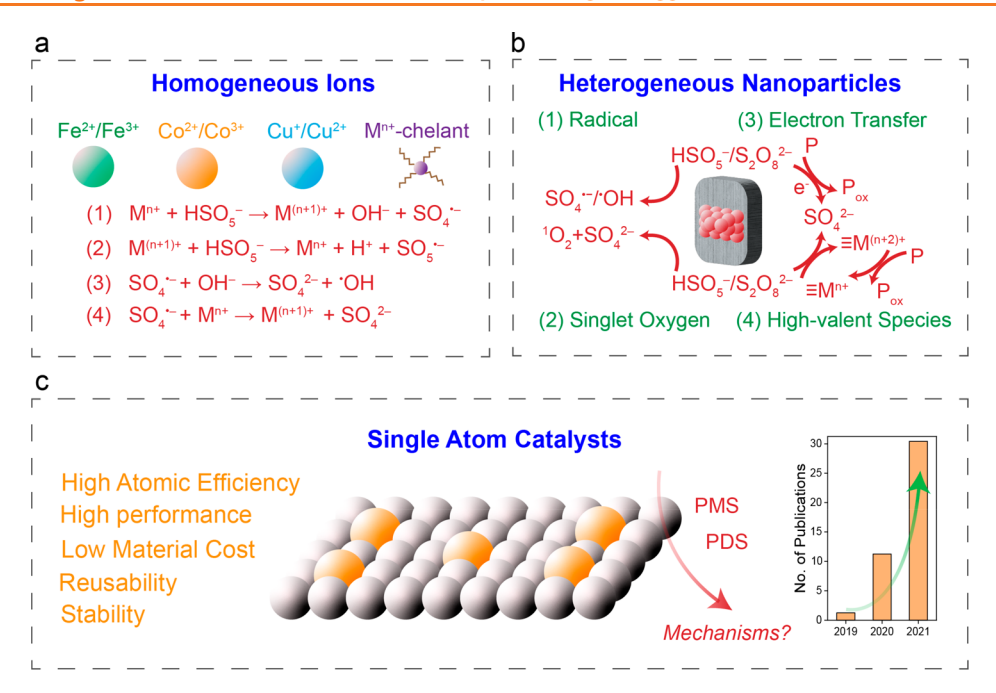


Figure 1. Schematic comparing (a) homogeneous ions, (b) heterogeneous nanoparticles, and (c) single atom catalysts for persulfate activation.

In comparison, heterogeneous metal nanoparticles have received great interest due to the ease of recycling the catalysts which are often immobilized onto a larger substrate (Figure 1b). The localized reaction on the substrate surface makes it possible to tune the reaction mechanisms, pollutant adsorption, and degradation kinetics via surface modification. Another advantage of loading catalysts onto conducting substrates is to enable AOPs electrochemically.²⁷ The mechanisms of persulfate activation by heterogeneous metal nanoparticles have been proposed to include mediated electron transfer in addition to mechanisms that are also found in homogeneous catalysis such as the radical pathway (SO₄ • and •OH), singlet oxygen (¹O₂) formation, and high-valent metal species induced oxidation. 28,29 However, nanoparticle catalysts suffer from relatively low atomic efficiency compared to homogeneous catalysis since a large fraction of metals are embedded within the particles instead of being exposed to reaction media and, therefore, cannot participate in the catalysis.

Single atom catalysts (SACs) have emerged as an alternative material architecture in recent years (Figure 1c) that retains the benefits of both homogeneous and heterogeneous catalysts. 30,31 The concept of SACs is to anchor metal catalysts on the substrate via strong ligand binding in an atomically dispersed fashion, eliminating metal-metal interactions and fully exposing each atom to the reaction media.³² Consequently, the 100% atomic efficiency of SACs mimics the homogeneous catalysts, while the presence of substrate enables facile recovery like heterogeneous catalysts. Due to the strong atomic interaction with the support, single atoms are generally more stable than their nanoparticle counterparts during chemical reactions.^{33–36} SACs have demonstrated extraordinary reactivity and selectivity in various reactions such as the oxygen reduction reaction (ORR),³⁷ hydrogen evolution reaction (HER),³⁸ and CO₂ reduction reaction (CO₂RR)³⁹ that are critical for energy and sustainability.

SACs have also been explored for catalytic pollution remediations including hydrodehalogenation, 40-42 oxyanion reduction, 43,44 and AOPs. 45-48 These interests were triggered

by a few uniquely advantageous features of SACs for environmental applications: (i) SACs achieve faster kinetics than nanoparticles when normalized per mass of catalysts; (ii) SACs are generally more cost-effective than nanoparticle counterparts, as they are often synthesized using similar methods with nanoparticles but using much less materials; (iii) SACs often exhibit enhanced reaction pathway selectivity, which is critical for the removal of target pollutants in a complex water matrix; (iv) SACs are typically more aqueous stable than nanoparticle counterparts due to the strong covalent bond with the substrate, lessening the environmental concern of material leaching; and (v) relatively simple and scalable synthesis of many SACs on various substrates, which can be readily executed by environmental scientists who have gained experience in nanomaterial synthesis and characterization over the past couple of decades. A prospect to realize these benefits has triggered recent attention on employing SACs for heterogeneous AOPs, persulfate-AOPs in particular.

However, realizing all the above foreseen benefits has a long way to go, since SAC research overall is still at an early phase. An increasing number of studies were published in the past few years, mostly focusing on synthesizing new SAC materials for persulfate-AOPs (Figure 1c inset and Table S1) and including literature reviews on recent progress with SAC-persulfate AOPs. 49-51 We recognize that there are still uncertainties and different views on the mechanisms of persulfate activation by SACs, especially the differences between SACs and nanoparticles. We here examine past literature to first review the methods and techniques that have been employed to synthesize and characterize SACs and their application toward persulfatebased AOPs. We then further our discussion on detailing various SAC-persulfate interaction mechanisms, particularly built around the mechanisms on how persulfate would interact with SACs differently from nanoparticle counterparts. We conclude our critical review by discussing existing challenges and proposing some critical research directions to further advance this technology.

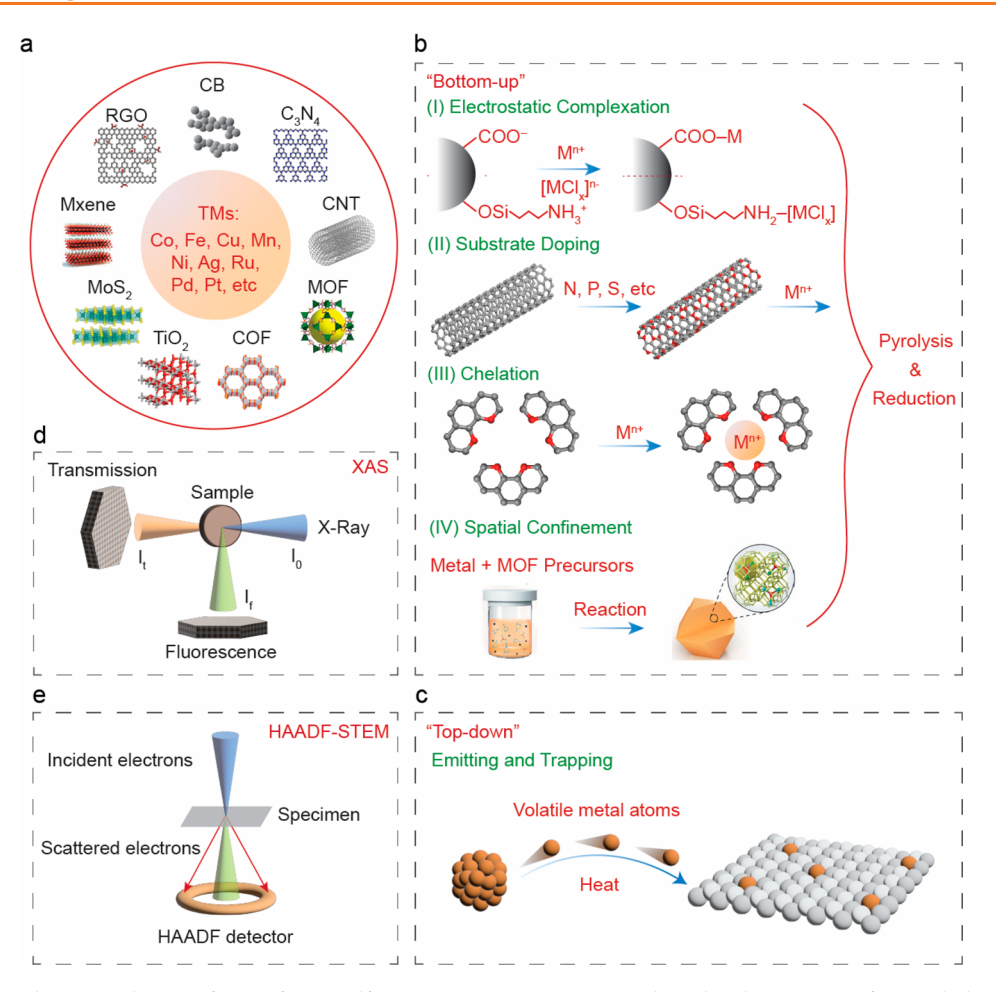


Figure 2. (a) Metal and support choices of SACs for persulfate-AOPs. MXene structure: adapted with permission from VahidMohammadi et al.¹³¹ Copyright 2021, The American Association for the Advancement of Science. MoS₂ structure: adapted with permission from Ghim et al.¹³² Copyright 2021, American Chemical Society. MOF structure: adapted with permission from Ding et al.¹³³ Copyright 2017, Wiley-VCH. COF structure: adapted with permission from Côté et al.¹³⁴ Copyright 2005, The American Association for the Advancement of Science. (b) "Bottom-up" SAC synthesis methods. The "spatial confinement" schematic: adapted with permission from Chen et al.¹³⁵ Copyright 2017, Wiley-VCH. (c) "Top-down" SAC synthesis methods. (d) Schematic illustrating XAS working principles. (e) Schematic illustrating HAADF-STEM working principles.

SAC SYNTHESIS AND CHARACTERIZATIONS

Metal and Support Choice. Similar to nanoparticles used for persulfate activation, transition metals (TMs) are commonly used for SACs, including Co, 40,52-56 Fe, 34,57-60 Cu, 61,62 Mn, $\text{Ni,}^{63} \text{ Ag,}^{64} \text{ and } \text{Ru}^{65} \text{ (Figure 2a)}.$ Cobalt and iron are the two most studied SACs for persulfate activation due to their proven catalytic activities. Noble TMs such as Pd and Pt can also activate persulfate²⁸ but have rarely been studied in the form of SACs. Carbon-based materials are commonly used as substrates to host SACs, since they provide ample anchoring sites (e.g., surface defects, vacancies) and their surface properties can be tuned by functionalization, heteroatom doping, coating, and/or hierarchical structuring to improve binding. The relatively high electrical conductivity of saturated carbon materials can also facilitate the electron transfer through the catalytic site, which is beneficial for persulfate activation by mediated electron transfer (discussed below).66,67 Examples include graphitic carbon, 56,57,68 reduced graphene oxide (rGO),61 carbon nitride (C_3N_4) , 52,64,69,70 carbon nanotubes (CNTs), 59 MXene, 71 metal organic frameworks (MOFs) such as zeolitic imidazolate framework (ZIF), 60,72,73 covalent organic frameworks (COFs),⁷⁴ and biochar.^{34,62} The electronic properties (e.g., conductivity), surface functional groups, and physical structures

(*e.g.*, from one to three dimensions) of these carbon supports have been shown to affect SAC-persulfate interactions. ^{49,59,75,76} Besides carbon-based supports, semiconductors such as TiO₂⁷⁷ and MoS₂⁷⁸ have also been employed for SAC-enhanced photocatalytic activation of PMS. Other materials such as metal oxides (*e.g.*, MgO, FeO₂, ZnO, WO₃, CuO, Co₃O₄, Al₂O₃, CeO₂)⁷⁹ and metal nanoparticles⁸⁰ have been widely used to support SACs in various application fields but not yet for the SAC-persulfate system.

SAC Synthesis Methods. We here briefly summarize methods to synthesize SACs, while a more comprehensive review can be found in previous literature. SACs synthesized by some of these approaches have been applied for persulfate AOPs, while many other approaches remain unexplored. In general, two strategies have been used in fabricating SACs: the "bottom-up" and the "top-down" approaches. The key difference between these two approaches lies in whether a mononuclear metal or a metal nanoparticle is used as the precursor. SP

The bottom-up approach is more widely used, as it ensures that each atom is intrinsically separated from the beginning. Mononuclear metal precursors are loaded onto the support via adsorption, complexation, chelation, or $\pi-\pi$ stacking, typically using wet chemistry, and then followed by final high-temper-

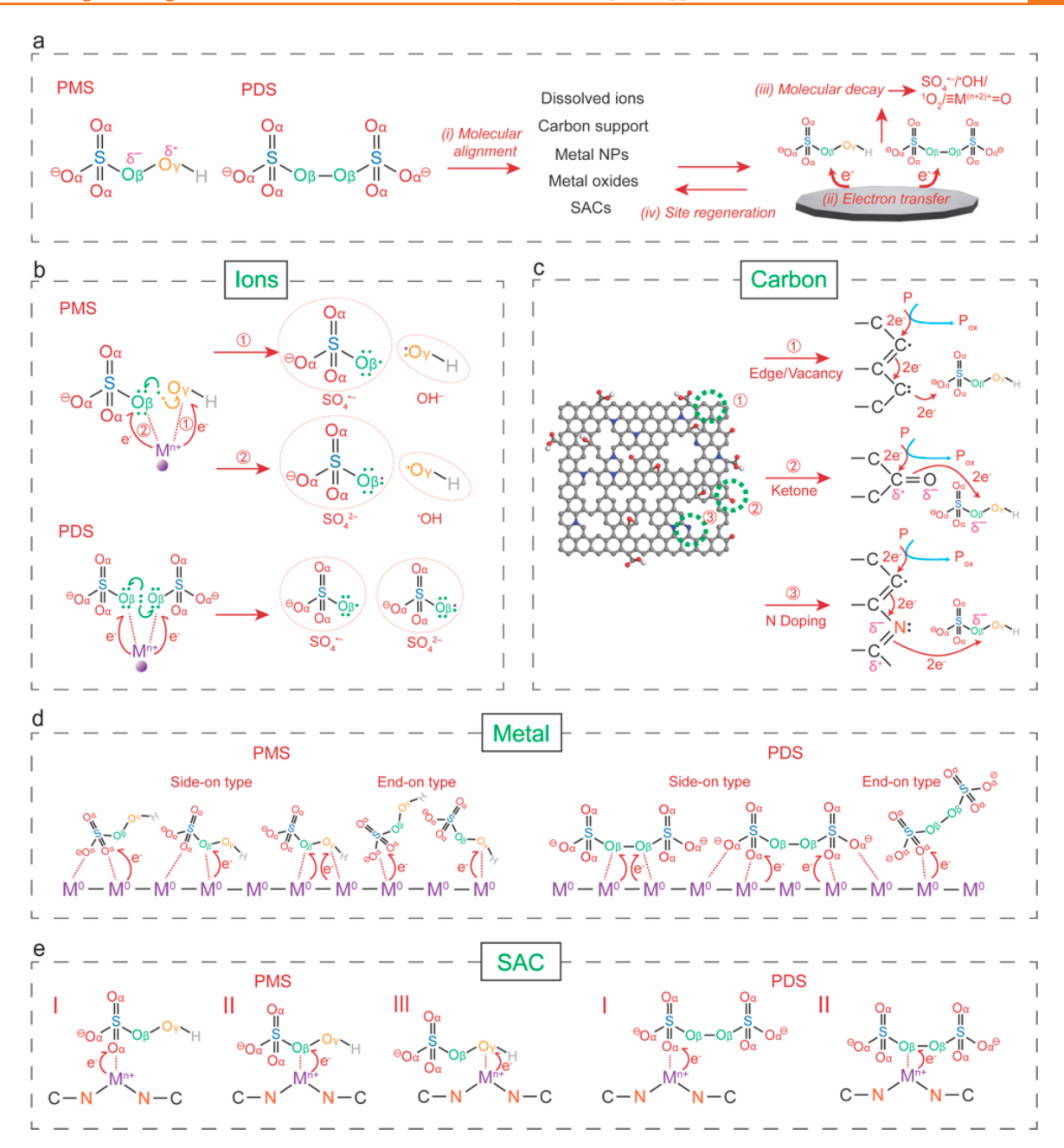


Figure 3. (a) Four-step reactions of persulfate activation by catalysts. (b-e) Persulfate molecular interaction with (b) dissolved metal ions, (c) carbon supports, (d) metal surfaces, and (e) SACs.

ature pyrolysis⁹⁰ or room temperature reduction by reducing chemicals^{91,92} or irradiation^{93,94} (Figure 2b). To avoid the aggregation of single atoms, a low weight percentage of metal over support is used (typically <1%). Several strategies have, therefore, been developed to increase metal loading:

(i) Electrostatic Interaction. Some supports intrinsically have a large number of surface functional groups which can serve as SAC binding sites. For example, at pH > pH_{iep}, GO's abundant negatively charged carboxylic groups (COO⁻) can anchor positively charged TM ions. SAS another example, negatively charged 2D $\text{Ti}_3\text{O}_7^{2-}$ in the titanate precursor effectively binds with $[\text{Pt}(\text{NH}_3)_4]^{2+}$, a precursor for Pt SACs. SAS The substrate can also be modified with surface linkers to offer better electrostatic interactions with metal precursors. For example, aminosilane is widely

- used to modify surfaces containing hydroxyl groups to be positively charged for binding with negatively charged metal precursors. 41,97,98
- (ii) Substrate Doping. Doping a substrate with N, P, and S with lone pairs of electrons can increase the coordination capability of the substrate toward metal precursors. 99,100 For example, Pt single atoms have been anchored onto N-doped CNT via the strong coordination interaction of the H₂PtCl₆·6H₂O precursor with hetero N atoms. 100
- (iii) Chelation. Metal ions can be chelated with organic ligands such as phthalocyanine, porphyrin, ortho-phenylenediamine, and phenanthroline to form organometallic complexes (i.e., analogous to homogeneous catalysts), 101-104 which can then either undergo direct pyrolysis to form carbon-SAC hybrids 102 or be loaded

onto other carbon supports such as carbon black or CNTs via π – π stacking interaction. ^{103,104}

(iv) *Spatial confinement.* The vacancy structure of MOFs and COFs can serve as a template to confine SACs and avoid their aggregation due to surface migration. ^{105,106}

In the top-down approach, metal—metal bonds in metal nanoparticle precursors are broken down by acid washing, 107,108 electrical corrosion, 109,110 or high-temperature treatment (typically >800 °C) $^{36,111-114}$ to form single atoms on the same support. Alternatively, an emitting-and-trapping strategy has been utilized to volatilize metal nanoparticles to single atoms, which are then trapped on a separate support (Figure 2c). The support that traps volatile metal atoms possesses abundant coordination sites or defects to form stable binding with the metal atoms that pass by. An oxidizing atmosphere (O $_2$ or air) is often preferred to form oxidative metal species. Ammonia atmosphere can also induce the formation of volatile metal-NH $_3$ complexes via Lewis acid—base interactions. 112,113

Characterization. X-ray absorption spectroscopy (XAS) is considered essential to determine SACs' oxidation states and coordination environments and consequently confirm their atomically dispersed states (Figure 2d). 115 In contrast, X-ray photoelectron spectroscopy (XPS), although it is widely used to evaluate the oxidation states of metals in nanoparticles, is generally not suitable for SAC analysis, since the beam energy (e.g., 5 keV with a top-notch Cr K α source) is too low for the low metal content in typical SAC samples (e.g., <1 wt %). XAS is also often operated in a fluorescence mode (i.e., in contrast to transmission mode), which is suitable to low metal loading (<3– 5 wt %). X-ray absorption near-edge structure (XANES) analysis provides information as to the oxidation states of metal atoms from the white-line intensities and the edge energies. 116 Extended X-ray absorption fine structure (EXAFS) analysis provides information on the coordination environment of metal atoms, ¹¹⁷ often in comparison to bulk metal, metal oxide, metal-N (*e.g.*, M-Pc), and/or sulfide references. ¹¹⁸ However, it is generally difficult to distinguish low-atomic-number elements such as C, N, O, and S from other similar elements. 119 Further curve fitting of EXAFS spectra based on standards provides the coordination number and bond length. The Debye–Waller factor needs to be considered in the EXAFS analysis to account for the disorder from static and/or thermal origin, which limits the accuracy of coordination numbers to be approximately ±20%. Another frequently used method to confirm the occurrence of SACs is in situ Fourier-transform infrared spectroscopy (FTIR) using CO as a probe molecule. 120 The CO adsorption signal on an SAC appears as one sharp interaction peak (one CO on one metal atom). 121 For nanoparticles, the peak becomes wider with additional bridging peaks (one CO on two contiguous metal atoms). 122 In either case, CO adsorption on substrates such as carbon material could complicate the interpretation. 123,124

A visual confirmation using scanning tunneling microscopy (STM) and high-angle annular dark-field scanning transmission electron microscopy (HAADF-STEM) is another essential technique to verify the presence of SACs. STM is commonly used to characterize SACs on a secondary metal support (*i.e.*, single atom alloy, SAA). ^{125–127} HAADF-STEM (Figure 2e) ⁸¹ is used when SACs are loaded onto substrate with lighter elements such as carbon, since the image intensity from each metal atom is approximately proportional to the square of its atomic

number. ¹²⁸ Aberration correction of HAADF-STEM (AC-HAADF-STEM) further enhances the contrast and resolution by focusing the electron beam <1 Å. ¹²⁹ Since the area surveyed by these high-resolution imaging techniques is extremely small, a complementary analysis using lower-resolution TEM needs to be carried out to fully exclude the possibility of nanoparticle/nanocluster formation over a larger area. Besides the abovementioned techniques, other methods, such as XPS, Raman spectroscopy, X-ray powder diffraction (XRD), and Mössbauer spectroscopy, are typically employed to obtain complementary information on the structures and properties of SACs and their host substrates. ^{85,130}

■ PERSULFATE INTERACTION

Reaction Steps of Persulfate Activation. To examine whether SACs can be an effective persulfate activator, it is important to understand how persulfate interacts with catalysts at the molecular level (Figure 3a). The different modes of such interaction lead to different persulfate activation pathways and kinetics. The first step of persulfate activation is the adsorption of the persulfate ion onto the catalytic site at varying molecular alignments (i.e., depending on which O atom of persulfate binds with the metal atom). The second step involves either one or two-e transfer from the catalyst to persulfate. Unlike the activation by external energy sources such as photons (UV photolysis) or heat (thermolysis), the activation of persulfate ions by metal catalysts involves electron transfer, which is the key driving force to weaken the O-O bond. The third step is molecular decay in which the electron transferred to the persulfate ion eventually results in the breakage of the O-O bond and the formation of reactive species such as radicals, ${}^{1}O_{2}$, and high-valent metal species ($\equiv M^{(n+2)+} = O$). The fourth step is the detachment of surface-adsorbed persulfate decay intermediates or products (e.g., moieties including SO₄*, *OH, O*, where the asterisk denotes species which can be either radical or anion) from the catalytic site and its

We first define O atoms of persulfate molecules under different categories (Figure 3a). 40,136 PMS (HSO₅⁻, p K_{a2} = 9.3¹³⁷) contains three types of O atoms: O_{α} : three terminal O atoms bonded to the S atom; O_{β} : one O atom bonded to both the S atom and another O atom; and O_{γ} : the O atom at the peroxide terminal, bonded to the H atom. The three O_{α} atoms are in resonance, sharing a pair of delocalized electrons, and have a relatively short S-O_{α} bond distance (1.435-1.444 Å). The S-O_{β} distance is 1.632 Å, and the O_{β}-O_{γ} bond distance is 1.460 Å. ¹³⁸ PDS (S₂O₈²⁻, pK_{a2} = -3.5¹³⁹) contains two types of O atoms: O_{α} : six terminal O atoms bonded to S atom; and O_{β} : the two O atoms bonded to both S and O atoms. The bond distances are 1.427 Å for S–O_{α}, 1.644 Å for S–O_{β}, and 1.497 Å for O_{β} – O_{β} . The breakage of peroxide bonds—*i.e.*, the O_{β} – O_{γ} bond (estimated dissociation energy = 140-213.3 kJ·mol⁻¹) in PMS and the O_{β} - O_{β} bond (dissociation energy = 140 kJ·mol⁻¹) in PDS—is the key process leading to radical generation. 140–142 However, they are different in that the O_{β} - O_{γ} bond in PMS is asymmetrical with a partial positive charge on the O₂, while the O_{β} - O_{β} bond in PDS is symmetrical. ¹⁴¹

Persulfate Molecular Interaction with Dissolved Ions and Carbon Supports. Electronegative O atoms in persulfate can coordinate with positively charged metal ion to form a complex (Figure 3b). Subsequent electron transfer from the complexed metal ion to the persulfate molecule due to the stronger electronegativity of O ($\chi_{\rm O}$ = 3.44) than TMs ($\chi_{\rm TM}$ =

1.36–2.54) leads to the breakage of the O–O bond and subsequent formation of radicals. Due to the asymmetrical $O_{\beta}-O_{\gamma}$ bond in PMS, the metal ion (Mⁿ⁺) can donate one e $^-$ to either O_{γ} (pathway $^{\textcircled{1}}$) or O_{β} (pathway $^{\textcircled{2}}$) atom, forming $SO_4^{\bullet-}/OH^-$ or $SO_4^{2-}/^{\bullet}OH$, respectively (Figure 3b). In comparison, the complex of Mⁿ⁺ with symmetrical PDS only leads to a pathway which generates one $SO_4^{\bullet-}$ and one SO_4^{2-} per PDS molecule.

The adsorption of persulfate ions on carbon supports has been extensively studied using density functional theory (DFT) simulations. $^{143-147}$ At the edge of the basal planes of 2D carbon materials such as GO, unsaturated carbons with spins of nonbonding σ or π electrons exist in large numbers due to bond termination and play a significant role in electron transfer toward adsorbed oxygen atoms in persulfate (Figure 3c, ①). $^{148-151}$ Consequently, carbon defective edges and vacancies were shown to be more reactive than the basal plane to activate persulfate molecule due to more efficient electron transfer from pollutants to persulfate. 143

In addition, electron-rich ketone and quinone groups have been suggested as major active sites among the O functionalities (carbonyl, carboxylic, and hydroxyl) on carbon supports, 143,146 similar to ORR reactions. 152,153 The C atom in the C=O structure serves as a binding site for persulfate, forming an O^-C^+-O^- bridge (Figure 3c, ②). 154 Interestingly, a higher O content usually leads to inferior PMS catalytic activities, including CNTs and GO, 143,146,155 which has been partially ascribed to the interference of the PMS molecular alignment with edge sites by steric hindrance when they are occupied by more O groups. 143 In addition, once these unsaturated carbons are occupied by O functionalities, the conductivity of the support decreases as the number of unpaired π -electrons decreases, 156 leading to less efficient electron transfer.

The doping of other heteroatoms, especially N (e.g., graphitic, pyridinic, and pyrrolic N), can help increase the adsorption of persulfate ions. ¹⁴⁴ The N doping tailors the charge distribution of adjacent carbons due to its higher electronegativity ($\chi_N = 3.04$ vs $\chi_C = 2.55$). Consequently, O atoms in persulfate more efficiently coordinate with partially positive carbons. The charge is then expected to transfer from the electron-rich N to persulfate molecules via the N⁻-C⁺-O⁻ bridge (Figure 3c, ③). ¹⁴⁴ Compared with O, the steric hindrance effect of N atoms on persulfate adsorption may be less significant since they are doped within the basal plane. Yet, similar to O, the effects of higher loading of N on the support's electron transfer and persulfate activation should be further investigated, as previous studies showed that an extensive N loading would lead to conductivity loss of carbon supports. ^{157–159}

Persulfate Molecular Interaction with Metal Nanoparticle, Oxide, and SAC. Researchers have been employing DFT for the past few years to establish the pathways of the persulfate activation with the focus on how the initial O atom alignment dictates the overall mechanism. It is noteworthy that, in the ORR, a similar reductive process as persulfate activation, the focus on the O₂ molecular alignment on the catalyst site has been widely studied in the past decade. We build our discussion on this analogy between persulfate activation and the ORR. The binding of O atoms in dioxygen on the metal surface is generally classified into three types: end-on Pauling-type (one O with one metal), side-on Griffiths-type (two O with one metals). The side-on types indicate strongly chemisorbed coordination, while the end-on type can be either

weakly chemisorbed or physiosorbed. These three different adsorption configurations determine how strongly the molecule is adsorbed on the catalytic site and how difficult it is for the intermediate to be released and for the catalytic site to be regenerated, thus affecting the overall activation pathway.

In persulfate interaction with metal or metal oxide NPs (Figure 3d), the side-on type has been simulated as a dominant adsorption mode of PDS on ${\rm Co_3O_4}$, 166 PMS on ${\rm CuCo_2O_4}$, 167 PMS on the (100) surface of ${\rm Cu_2O_1}^{168}$ PMS on Co NPs and ${\rm CoO_1}^{46}$ and PMS on ${\rm Fe_2O_3}$. 169 Some studies also elaborated on the end-on type, such as PMS on the (110) and (111) surfaces of ${\rm Cu_2O_1}^{168}$ PMS on δ -MnO₂, 170 and PDS on NiO. 171 The crystalline phase, facet type, nanoparticle size, heteroatom doping, and solvent environment can all affect the thermodynamically favorable adsorption configuration of persulfate. 147,168 To date, DFT studies on metal or metal oxide NPs mainly target for simulating the mechanisms and confirming the O–O bond cleavage, while few of them considered different adsorption types and their thermodynamical/kinetic implication.

For persulfate interaction with SACs, in particular, SACs in the M–N_x–C structure, the end-on type has been simulated for both $PMS^{40,58,169,172-174}$ and $PDS^{175,176}$ as the major adsorption mode. The side-on type is usually not considered due to the fact that it requires two adjacent metal atoms. This is similar to the ORR, in which the adsorption of O₂ on SACs is typically end-on type, rather than side-on coordination. 165,177 Taking the $M-N_x-C$ structure as an example, with end-on type, as persulfate has different O types, its molecular alignment along the SACs can thus have several categories depending on which O atom is coordinated. The alignment can be defined into three categories for PMS: type I $(M-O_{\alpha})$, type II $(M-O_{\beta})$, and type III $(M-O_{\gamma})$ (Figure 3e); and two categories for PDS: type I $(M-O_{\alpha})$ and type II $(M-O_{\beta})$. For example, type I has been considered for PMS interaction with Fe-N $_4$ -C $^{58,169,172-174}$ In contrast, type $I^{46,172}$ and type III^{40} for PMS with Co-N₄-C and type I for PDS with Fe-N₄-C and Cu-N₂-C have also been assumed. 175,176 These different adsorption modes determine the electron transfer process and how strongly persulfate and intermediate species bind with the SAC and, therefore, the overall persulfate activation pathway. For example, it may affect whether the electrons transferred from the single atom Mⁿ⁺ go to the $-SO_4$ or the -OH within persulfate, affecting the available radical type.

Application of DFT for SAC-Persulfate Interaction **Analysis.** It is difficult to directly observe persulfate interaction pathways with SACs using conventional characterization techniques. In general, instrumental analysis can confirm the types of resulting reactive species but does not provide mechanistic insights for their generation pathways. Theoretical simulations such as DFT have, therefore, been frequently employed to analyze SAC-persulfate interaction pathways, including molecular alignment, electron transfer, and molecular decay. DFT calculation aims to validate the experimental results, determine the main active sites, evaluate thermodynamical and kinetic feasibilities, predict intermediates, and explore the effects of different factors (e.g., water chemistry, catalyst composition). The collective information is beneficial for guiding the design of more effective, robust, and sustainable SACs to achieve high atomic activity and selectivity in persulfate-based water treatments in the future.

DFT can suggest the most thermodynamically favorable pathway for each persulfate alignment mode based on the adsorption energies ($E_{\rm ads}$), the activation energy barrier (ΔG),

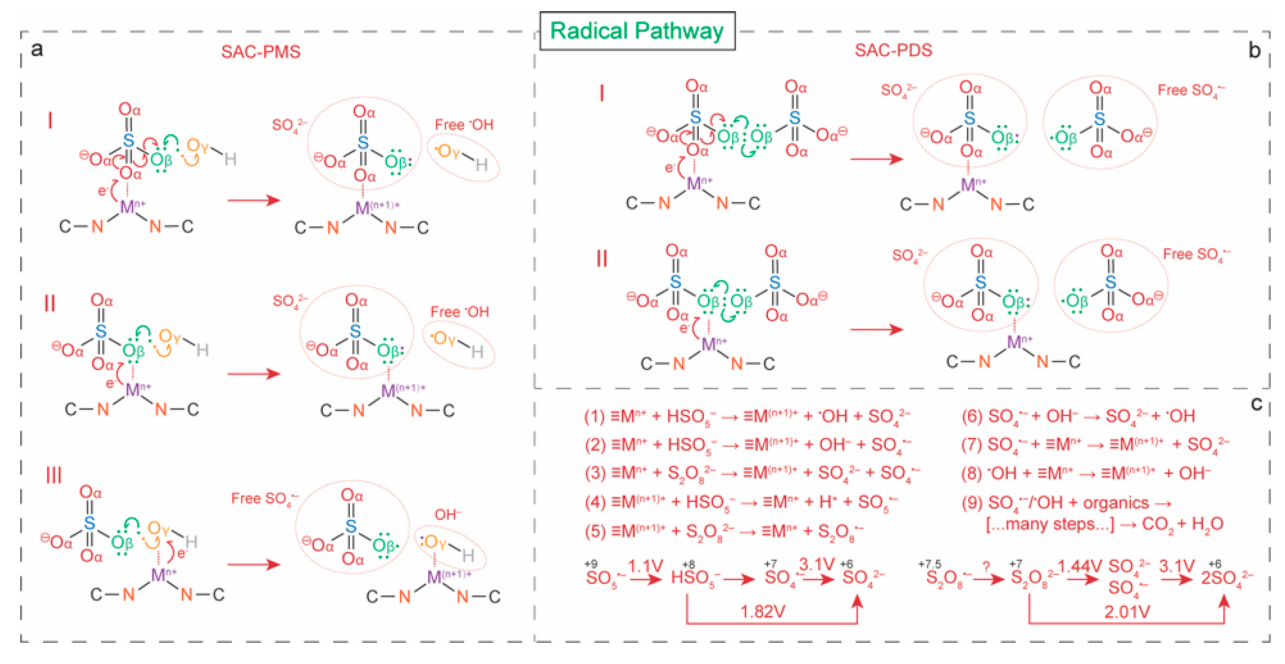


Figure 4. (a) Radical generation pathway of the SAC-PMS system. (b) Radical generation pathway of the SAC-PDS system. (c) Reaction steps in SAC-persulfate to generate radicals, and standard redox potentials (E^0) of the PMS and PDS reactions. 13,198

and the extent of O–O bond length elongation $(l_{\rm O-O})$. For example, DFT showed that type I would be more favorable than type II for PMS adsorption on Fe-N₄-C, 174 while type III would be more efficient than type II for PMS adsorption on Co-N₄-C, ultimately leading to elongation of the O-O bond and generation of SO₄• and •OH. ⁴⁰ DFT can also help explain the differences between SACs and other catalysts. For Fe-N₄-C and $Co-N_4-C$, 46,169,172 the relationship between the reaction kinetics and $E_{\rm ads}$ of PMS on various substrates follows a volcano shaped trend. In other words, while the binding strength is in the order of oxide \approx pure metal > M-N₄-C > graphitic N > carbon, the kinetics was fastest with $M-N_4-C$. This suggests that the binding between PMS and catalyst should be strong enough to facilitate PMS activation and subsequent activation (i.e., in contrast to weakly binding carbon), while it should be weak enough to avoid catalytic site poisoning by reaction intermediates (i.e., in contrast to strongly binding metal or metal oxide). In this example, this balance is achieved with SAC in the $M-N_4-C$ configuration.

Note that metal or metal oxide NPs interact with persulfate majorly through the side-on mode with more than one O atom binding to the metal, explaining the reason why the binding strength is higher than the end-on mode, which is the case of SACs. However, NPs' interaction with persulfate can also be the end-on type, 168,170,171 which might decrease binding energies. In the ORR, it was shown that when the Au NP size is smaller, more end-on Pauling-type of $\rm O_2$ adsorption occurs. 163 The adsorbed O atoms can turn from end-on Pauling-type into the side-on Griffiths-type gradually with time for Mn–N₄–C in the ORR. 178 Similar behavior might be possible with persulfate but has not yet been reported.

ELECTRON TRANSFER AND PERSULFATE MOLECULAR DECAY ON SACS

Radical Generation. A number of studies have identified radicals (SO₄ • and •OH) as the main product of persulfate activation by SACs. ^{40,47,52,57,64,179–181} To verify the radical

generation pathway, researchers have employed two experimental approaches: the scavenging experiment and the electron paramagnetic resonance (EPR) analysis for indirect and direct confirmations, respectively. Radical scavengers such as methanol (MeOH, $k_{\text{SO4}\bullet-/\text{MeOH}} = 3.2 \times 10^6 \text{ M}^{-1} \text{ s}^{-1}$, $k_{\bullet \text{OH/MeOH}} = 9.7 \times 10^8 \text{ M}^{-1} \text{ s}^{-1}$) or ethanol (EtOH, $k_{\text{SO4}\bullet-/\text{EtOH}} = (1.6-7.7) \times 10^7 \text{ M}^{-1} \text{ s}^{-1}$, $k_{\bullet \text{OH/EtOH}} = (1.2-2.8) \times 10^9 \text{ M}^{-1} \text{ s}^{-1}$) can be used to quench both SO₄ and OH. In contrast, *tert*-butanol (TBA, $k_{\text{SO4}\bullet-/\text{TBA}} = (4-9.1) \times 10^5 \,\text{M}^{-1} \,\text{s}^{-1}, k_{\bullet \text{OH}/\text{TBA}} = (3.8-7.6) \times 10^9 \,\text{M}^{-1} \,\text{s}^{-1})$ or nitrobenzene (NB, $k_{\text{SO4}\bullet-/\text{NB}} < 10^6 \,\text{M}^{-1} \,\text{s}^{-1}, k_{\bullet \text{OH}/\text{NB}}$ = $(3.0-3.9) \times 10^9 \text{ M}^{-1} \text{ s}^{-1}$) can be used to nearly exclusively quench *OH. 182 A decrease in pollutant removal kinetics in the presence of a radical scavenger is used to gauge the relative role of a particular radical. For EPR, 5,5-dimethyl-1-pyrroline Noxide (DMPO) is commonly used as a spin-trapping agent for both *OH and SO4*-, generating characteristic peaks of DMPO•OH and DMPO•SO₄, respectively, ^{52,57,71,180,183} or 5,5-dimethyl-2-pyrrolidone-N-oxyl (DMPOX)^{34,40,47} which is formed by further radical-mediated oxidation of DMPO*-OH with $SO_4^{\bullet-.184}$ The main challenge of using DMPO for detecting $SO_4^{\bullet-}$ is the low water stability of DMPO $^{\bullet}$ -SO₄, since it easily reacts with H_2O/OH^- to form DMPO $^{\bullet}$ -OH ($t_{1/2}$ of DMPO $^{\bullet}$ -SO₄ = 95 s in water¹²) and consequently the DMPO*-SO₄ peak intensity decreases over time.

In the radical pathway, similar to dissolved metal ion-persulfate interactions, one electron is transferred from the single metal atom site to the coordinated O atom of the persulfate molecule due to the stronger electronegativity of O than TMs. This one-electron transfer leads to bond elongation and breakage of the O–O bond, generating either SO₄*- or *OH. *40 For PMS, type I and II adsorptions lead to the formation of a surface-bound SO₄*- and a free *OH radical, while type III leads to the formation of a surface-bound OH⁻ and a free SO₄*- radical (Figure 4a). The oxygen that is coordinated with the single atom receives one electron, forming anions (SO₄*- or OH⁻), while the other side is released in the form of free radicals (SO₄*- or *OH) (reactions (1) and (2), Figure 4c). For PDS

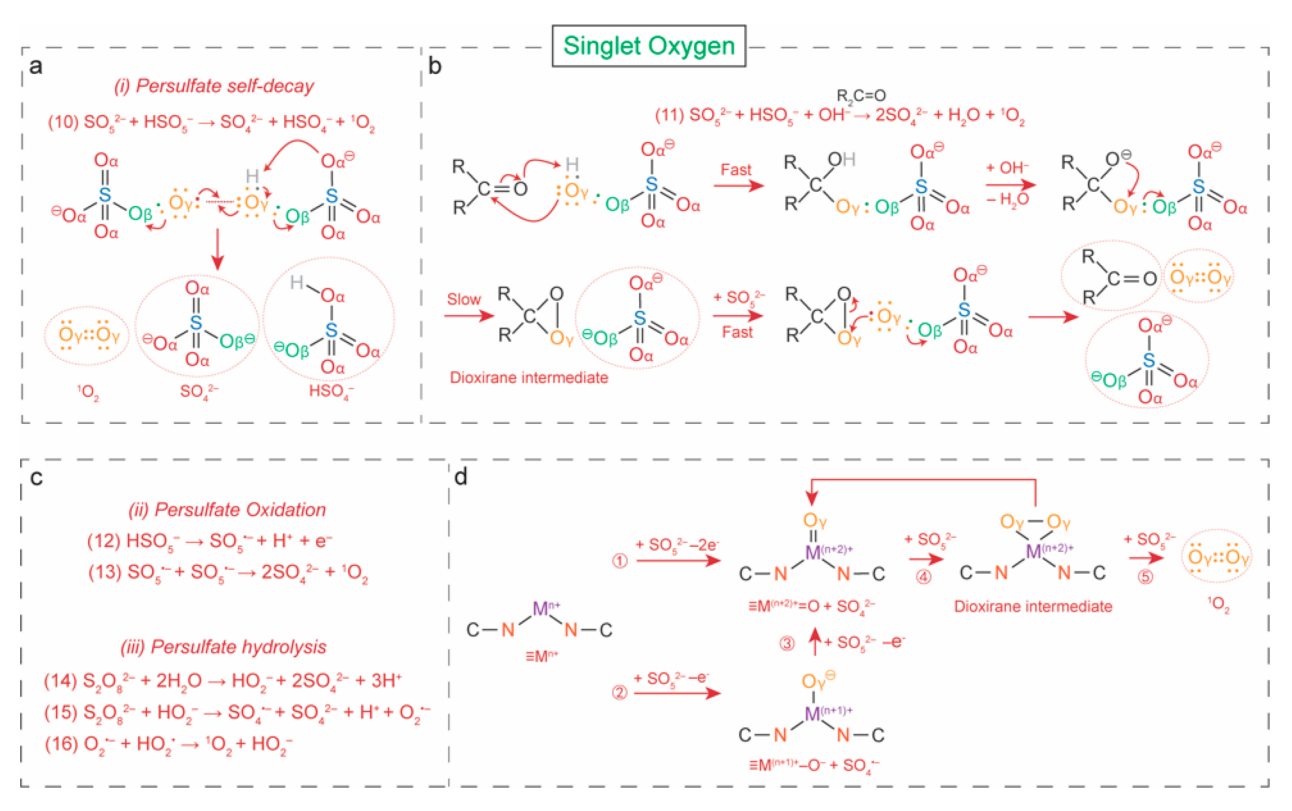


Figure 5. (a) Self-decay pathway from PMS to generate $^{1}O_{2}$. (b) Pathway of $^{1}O_{2}$ generation from catalyzed PMS self-decay by $R_{2}C$ =O groups on carbon supports. (c) Persulfate oxidation and hydrolysis pathways to form $^{1}O_{2}$. (d) Proposed $^{1}O_{2}$ generation pathway in the SAC-PMS system.

(Figure 4b), types I and II all lead to the formation of a surface-bound SO_4^{2-} and a free $SO_4^{\bullet-}$ radical (reaction (3)).

For PMS, it is noteworthy that the types of free radicals generated depend on the PMS alignment configuration. However, this may not necessarily dictate which radical, SO₄ or OH, plays the most dominant role in pollutant degradation, as it also depends on the reactivity, selectivity, and lifetime of the radical. For example, ${}^{\bullet}OH$ has approximately 1–2 orders of magnitude higher second-order rate constants (M⁻¹ s⁻¹) than SO₄•- toward alcohols, acids, and aromatics, ⁵ despite the 2-4 orders of magnitude shorter lifetime than $SO_4^{\bullet-}$. In addition, the selectivity of OH is lower than $SO_4^{\bullet-}$ as it is highly reactive and can be scavenged by abundant inorganic anions in wastewater including chloride, bicarbonate, bromide, iodide, and nitrite. Other chain reactions can also affect the availability of $SO_4^{\bullet-}/^{\bullet}OH$ such as quenching of $SO_4^{\bullet-}$ by OH^- from water (reaction (6)) and the reaction of $SO_4^{\bullet-}$ or ${}^{\bullet}OH$ with $\equiv M^{n+}$ to form $\equiv M^{(n+1)+}$ (reactions (7) and (8)). 24,185

From the perspective of the metal single atom ($\equiv M^{n+}$), during the one-e charge transfer process, $\equiv M^{n+}$ becomes oxidized to form $\equiv M^{(n+1)+}$, similar to the case of homogeneous catalysis. So Once the surface-bound SO_4^{2-} or OH^- detaches, the $\equiv M^{(n+1)+}$ can be reduced back to $\equiv M^{n+}$ by the persulfate molecule to complete the redox cycle (reactions (4) and (5)). As far as we know, the reduction of $\equiv M^{(n+1)+}$ to $\equiv M^{n+}$ by PMS or PDS has not yet been experimentally confirmed. The redox potentials of common $\equiv M^{n+}/\equiv M^{(n+1)+}$ groups are Co^{3+}/Co^{2+} ($E^0 = 1.82$ V), Fe^{3+}/Fe^{2+} ($E^0 = 0.77$ V), Cu^{2+}/Cu^{4-} ($E^0 = 0.17$ V), Mn^{3+}/Mn^{2+} ($E^0 = 1.51$ V), and Ag^{2+}/Ag^{4-} ($E^0 = 1.98$ V). The redox potentials of PMS oxidation are SO_5^{-}/HSO_5^{-} ($E^0 = 1.1$ V) and SO_5^{-}/SO_5^{2-} ($E^0 = 0.81$ V) (Figure 4c). The E^0 value of $S_2O_8^{-}/S_2O_8^{2-}$ is not yet available in the literature. Thermodynamics suggest that the oxidation of

 ${\rm HSO_5}^-$ by ${\rm Fe^{3+}}$ and ${\rm Cu^{2+}}$ is difficult, while ${\rm Co^{3+}}$, ${\rm Mn^{3+}}$, and ${\rm Ag^{2+}}$ can be readily reduced by ${\rm HSO_5}^-$.

The ${\rm S_2O_8^{2-}}$ oxidation by $\equiv M^{(n+1)+}$ (reaction (5)) is still in

debate. Some claimed that it is not thermodynamically favorable under the environmental conditions, ^{13,14} while others proposed this reaction can occur with Fe(III)- and Mn(IV)-containing oxides. 187,188 One challenge for confirming the formation of $S_2O_8^{\bullet}$ is that it easily reacts with dissolved oxygen, H_2O_7 , or \equiv $M^{2(n+1)+}$. 189 Transient absorption spectra or EPR has been used to identify $S_2O_8^{\bullet-}$, but their accuracy is questionable, since there is no standard reference to compare. 190,191 Some studies also proposed that the metal redox cycle can be completed by electron transfer from pollutant degradation intermediates (≡ $M^{(n+1)+}$ + pollutant intermediates $\rightarrow \equiv M^{n+}$). $^{192-194}$ Co³⁺, Mn³⁺, and Ag^{2+} can also be reduced by H_2O ($E^0(O_2/H_2O)$) = 1.23 V). In the future, the active $\equiv M^{n+}$ site regeneration pathway during persulfate activation by SACs and counterparts should be more carefully studied using in situ valence state characterization techniques and computational simulations. This is an important aspect, as it determines whether the catalyst can continuously perform in the long term, and whether external auxiliary reduction approaches (e.g., electric cathodic reduction, 195 chemical reductants such as hydroxylamine 196,197) should be used to assist the metal redox cycle completion.

 $^{1}\text{O}_{2}$ **Generation Pathway on SAC.** Singlet oxygen is another commonly observed ROS in persulfate activation systems. Several studies have found that $^{1}\text{O}_{2}$ was the main contributor in SAC-persulfate systems, 46,74,199,200 and some observed that almost 100% PMS was converted to $^{1}\text{O}_{2}$ on single atom sites. S4,174,201 Similar with previous nanoparticle or oxide persulfate systems, $^{1}\text{O}_{2}$ scavengers including NaN₃ ($k_{102/\text{NaN3}} = 1 \times 10^{9} \, \text{M}^{-1} \, \text{s}^{-1}$), furfuryl alcohol (FFA, $k_{102/\text{FFA}} = 1.2 \times 10^{8} \, \text{M}^{-1} \, \text{s}^{-1}$), or L-histidine ($k_{102/\text{L}}$ -histidine = 3.2 × 10⁷ M⁻¹

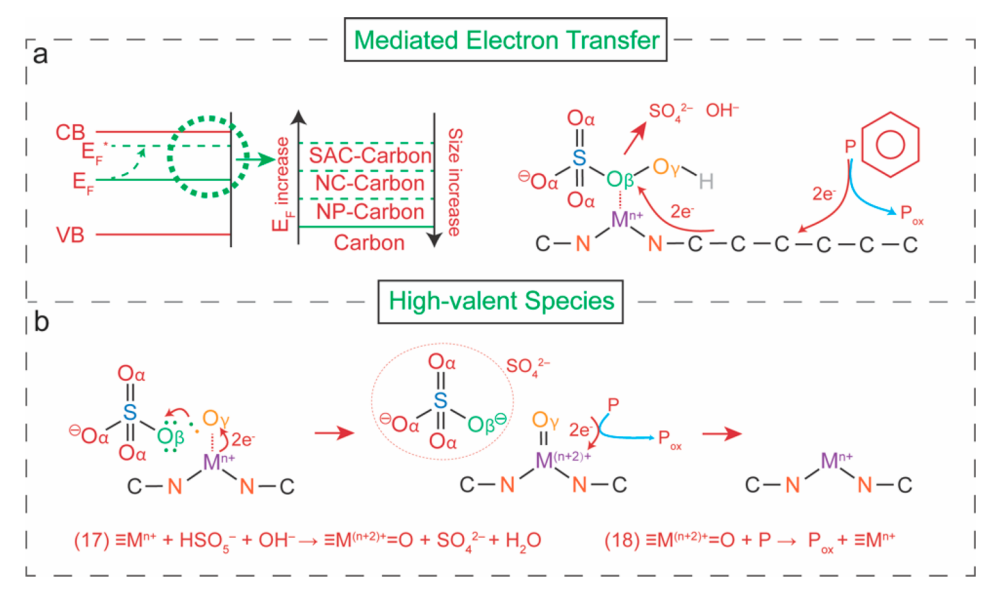


Figure 6. (a) Mediated electron transfer in the SAC-persulfate system. (b) High-valent species generation in the SAC-persulfate system.

 s^{-1}), $rac{202}{3}$ are used to identify the contributing roles of $rac{1}{0}$ in SACpersulfate systems. However, we would like to point out that these three scavengers also rapidly react with PMS. For example, it was shown that 10 mM NaN3 and L-histidine caused the complete decomposition of 1 mM PMS in 30 min, and 100 μ M FFA led to 30% degradation of 1 mM PMS after 175 min. 203 This suggests that when using these three scavengers, especially NaN₃ and L-histidine, the PMS decay over time should be taken into consideration to partially contribute to the inhibited pollutant degradation. In addition, *OH also reacts with these scavengers: $k_{\bullet \rm OH/NaN3} = 1.2 \times 10^{10} \, \rm M^{-1} \, s^{-1}, ^{204} \, k_{\bullet \rm OH/FFA} = 1.5 \times 10^{10} \, \rm M^{-1} \, s^{-1}, ^{203} \, k_{\bullet \rm OH/L}$ -histidine = $5.0 \times 10^9 \, \rm M^{-1} \, s^{-1}, ^{204}$ with 1-2 orders of magnitude higher k values than ${}^{1}O_{2}$. This posts another concern on using them as specific ¹O₂ scavengers in persulfate systems where OH exists. For EPR, 2,2,6,6tetramethylpiperidine (TEMP) is used as the trapping agent to capture ¹O₂. Strong triplet signals with an intensity ratio of 1:1:1 indicate the generation of ${}^{1}O_{2}$. The evidence of ${}^{1}O_{3}$. contribution can also be achieved by using deuterium oxide (D_2O) as the solvent. ²⁰² As the lifetime of 1O_2 in D_2O (22–70 μ s) is much longer than that in H₂O (2.9-4.6 μ s), ²⁰⁵ the degradation of pollutants would be enhanced after replacing H_2O by D_2O .

The aforementioned methods provide qualitative identifications of $^{1}O_{2}$. In order to quantify $^{1}O_{2}$ concentrations, 9,10-diphenylanthracene (DPA) has been widely used as a probe, 206,207 based on the rapid reaction with $^{1}O_{2}$ ($k_{1O2/DPA} = 1.3 \times 10^{6} \text{ M}^{-1} \text{ s}^{-1}$). 208 A stable DPA endoperoxide (DPAO $_{2}$ EPO) product can be measured using high-performance liquid chromatography (HPLC). Numerous other chemical probes have been employed for $^{1}O_{2}$, 209 which form an endoperoxide bridge structure (-O-O-) that exhibits unique (i) UV-vis absorption (*e.g.*, anthracenes modified with hydrophilic groups, 210 furans which are commercially available 211); (ii) photoluminescence (including 1,3-diphenylisobenzofuran (DPBF, $k_{1O2/DPBF} = 9.6 \times 10^{8} \text{ M}^{-1} \text{ s}^{-1}$), 212 modified anthracenes and tetracenes, 213 and commercial products such as the Singlet Oxygen Sensor Green, 214 AlphaScreen, 215 and AlphaLISA); 216 and (iii) chemiluminescence (including spirodioxetanes 217 and lanthanide complexes). 218 Future studies may consider comparing chemical probes to quantify $^{1}O_{2}$ concentrations

with and without pollutants and other potentially interfering species including reactive radicals.

Three common pathways have been proposed for ¹O₂ generation for persulfate activation by carbon or metal catalysts: (i) the catalyzed persulfate self-decay pathway (e.g., HSO₅⁻ + $SO_5^{2-} \rightarrow HSO_4^{-} + SO_4^{2-} + {}^1O_2$) (Figure 5a, reaction 10)²¹³,220 [In carbonaceous systems, the ketonic groups $(R_2C=O)$ are reported to accelerate the ¹O₂ formation from PMS self-decay at alkaline conditions with a dioxirane intermediate (Figure 5b, reaction 11). 154,220-222 Since the proton in the -OH part of PMS needs to be deprotonated to form ¹O₂ eventually, alkaline conditions are preferred.]; (ii) the persulfate oxidation pathway involving $SO_5^{\bullet-}$ radical $(HSO_5^- \to SO_5^{\bullet-} + H^+ + e^-; SO_5^{\bullet-} + SO_5^{\bullet-} \to 2SO_4^{2-} + {}^1O_2)$ (Figure 5c, reactions 12 and 13); 145,223,224 (iii) the hydrolysis pathway involving superoxide radical $(O_2^{\bullet}$ or HO_2^{\bullet} , $pK_a = 4.8$) $(e.g., S_2O_8^{2-} + 2H_2O \rightarrow HO_2^{-} + 2SO_4^{2-} + 3H^+; S_2O_8^{2-} + HO_2^{-} \rightarrow SO_4^{\bullet} + SO_4^{2-} + H^+ + O_2^{\bullet})$ (Figure 5c, reactions 14 and 15). Superoxide is believed to be an intermediate precursor for ¹O₂ through the proton-promoted disproportionation reaction $(O_2^{\bullet -} + HO_2^{\bullet} \rightarrow$ $^{1}O_{2} + HO_{2}^{-}$) (Figure 5c, reaction 16). ²²⁶ Benzoquinone (BQ), a selective radical scavenger of $O_2^{\bullet-}$ ($K_{O2\bullet-/BQ} = 2.9 \times 10^9 \text{ M}^{-1} \text{ s}^{-1}$), $K_{O2\bullet-/BQ} = 2.9 \times 10^9 \text{ M}^{-1} \text{ s}^{-1}$), $K_{O2\bullet-/BQ} = 2.9 \times 10^9 \text{ M}^{-1} \text{ s}^{-1}$), $K_{O2\bullet-/BQ} = 2.9 \times 10^9 \text{ M}^{-1} \text{ s}^{-1}$), $K_{O2\bullet-/BQ} = 2.9 \times 10^9 \text{ M}^{-1} \text{ s}^{-1}$), $K_{O2\bullet-/BQ} = 2.9 \times 10^9 \text{ M}^{-1} \text{ s}^{-1}$), $K_{O2\bullet-/BQ} = 2.9 \times 10^9 \text{ M}^{-1} \text{ s}^{-1}$), $K_{O2\bullet-/BQ} = 2.9 \times 10^9 \text{ M}^{-1} \text{ s}^{-1}$), $K_{O2\bullet-/BQ} = 2.9 \times 10^9 \text{ M}^{-1} \text{ s}^{-1}$), $K_{O2\bullet-/BQ} = 2.9 \times 10^9 \text{ M}^{-1} \text{ s}^{-1}$), $K_{O2\bullet-/BQ} = 2.9 \times 10^9 \text{ M}^{-1} \text{ s}^{-1}$), $K_{O2\bullet-/BQ} = 2.9 \times 10^9 \text{ M}^{-1} \text{ s}^{-1}$), $K_{O2\bullet-/BQ} = 2.9 \times 10^9 \text{ M}^{-1} \text{ s}^{-1}$. Note that in the catalyzed persulfate decay or oxidation, two O atoms in ¹O₂ originate from two separate PMS molecules, while, in the hydrolysis pathway, the two O atoms in ¹O₂ originate from H₂O

The mechanism of how SACs catalyze $^1\mathrm{O}_2$ generation remains to be established. Some recent DFT studies investigated the possible generation pathways of $^1\mathrm{O}_2$ on single atom sites. 174,201,228 For example, a metal—O complex structure, which results from the persulfate decay on the SAC site, was proposed to be an important intermediate in forming $^1\mathrm{O}_2$. 182,209 However, the exact configuration of this metal—O complex structure is unknown and needs more experimental or theoretical validation. It is possible that the SAC may catalyze persulfate self-decay through a metal—dioxirane intermediate pathway (Figure 5d), analogously to the generation of $^1\mathrm{O}_2$ on ketonic groups on carbon supports. First, PMS molecular

adsorption on the SAC site ($\equiv M^{n+}$) can lead to the formation of $\equiv M^{(n+2)+} = O$ through two-e⁻ transfer (①) or consecutive one-e⁻ transfers (② and ③). The $\equiv M^{(n+2)+} = O$ then acts similarly as $R_2C=O$, catalyzing 1O_2 generation from PMS decay with a metal—dioxirane intermediate (④ and ⑤). If this hypothesis is true, this mechanism may explain why 1O_2 was reported to be predominant in some SAC-persulfate systems. 54,174,201 As compared to nanoparticle counterparts, SACs may be more prone to form the $\equiv M^{(n+2)+} = O$ structure when reacting with peroxides.

It should also be pointed out that the reaction kinetics between $^1{\rm O}_2$ and many organic compounds ($k=\sim 10^2-10^8~{\rm M}^{-1}~{\rm s}^{-1}$), including phenolic and pharmaceutical compounds, are much slower than radicals ($k=\sim 10^6-10^{11}~{\rm M}^{-1}~{\rm s}^{-1}$) and more dependent on pH. Despite many recent studies that focus on promoting $^1{\rm O}_2$ generation from persulfate activation, including those that employ SAC as a catalyst, the relative ineffectiveness of $^1{\rm O}_2$ as a pollutant oxidant leaves a question mark over designing new persulfate systems with such focus.

Mediated Electron Transfer on SACs. A persulfate activation mechanism based on mediated electron transfer has been proposed for many nanoparticles^{28,229} and carbonaceous catalysts. ^{143,220,230} Similarly, it has been proposed also for SACs, ^{55,60,62,63,231} in which the electrons are transferred from the pollutant to the single atom site and further to the persulfate molecules (Figure 6a). Unlike the radical generation pathway in which persulfate abstracts one electron from the single atom site to form radicals, here persulfate abstracts two electrons from organic compounds to form sulfate ions with the single metal site serving as the electron transfer conduit.

Several complementary experiments can be carried out to verify this mechanism: (i) both the scavenging and the EPR tests prove the lack of radicals or $^1\mathrm{O}_2$; (ii) *in situ* Raman spectra show the peak of adsorbed peroxo species (*e.g.*, PMS* at around 830 cm $^{-1}$), confirming the PMS molecular binding on the catalyst surface; 60,62,63 (iii) the open-circuit potential (OCP) of the electrode loaded with catalyst shows a significant alteration after the addition of PMS and pollutant; 60,62 (iv) chronoamperometry (CP) measurements show that, at a certain applied voltage, the current through the catalyst increases when both PMS and pollutant exist. 60,62 Note that carbonaceous supports themselves are often conductive; it is thus important to isolate the role of metal catalysts. 63

SACs have been shown to possess enhanced metal-support interaction that facilitates charge transfer to/from substrate. 55,62,231,232 DFT is particularly useful in providing the electron density and charge accumulation surrounding the single atom site and at the SAC-substrate junction. An increased total density of states (TDOS)²³¹ around the Fermi level can reduce the interfacial Schottky junction barrier between the metal catalyst and the support and consequently induce more free electrons at the metal site.²³³ For SACs on carbons, studies suggested that the TODS near the Fermi level was higher for the M-N-C site than neighboring C or N atoms, with dominant contributions from the metal d orbitals (e.g., 3d for Fe, Co, Cu, Ni, 4d for Pd, Ag, and Ru, and 5d for Pt and Au). ^{233–235} Previous analysis also suggested that the Fermi level of SAC-loaded carbon shifted more negatively compared to pristine carbon supports (Figure 6a). 62,231 This is consistent with literature on nanoparticles where the Fermi level of smaller semiconductor particles would become more negative, i.e., closer to the conduction band and becoming a better electron donor.²³ Consistently, DFT suggested a higher charge accumulation

centered at the single atom site as well as between the single metal atom and coordinated-N(C), 55,232 which would facilitate persulfate reduction.

High-Valent Species Generations on SAC. High-valent metal-oxo species ($M^{(n+2)+}=O$), including Mn^{5+} , 23^7 Ru $^{5+}$, 23^8 Co $^{4+}$, 23^9 and Fe $^{4+}$, 240-242 have been reported as the main contributors in some dissolved metal ion or metal oxide/nanoparticle systems. Recently, the same species have also been proposed as the main contributors for Fe SACs using both experiments and DFT calculations (Figure 6b). $^{59,68,243-245}$ To identify the role of $M^{(n+2)+}=O$, sulfoxides such as methyl phenyl sulfoxide (PMSO) can be used. PMSO can be selectively oxidized to sulfones (*e.g.*, methyl phenyl sulfone, PMSO₂) by $M^{(n+2)+}=O$. 239 In addition, the ^{18}O isotope-labeling technique can be used to verify the existence of $M^{(n+2)+}=O$ via the oxygen atom exchange (OAE) reaction between $M^{(n+2)+}=O$ and $H_2^{18}O$. 239,246 Using $H_2^{18}O$ as the matrix, the ^{18}O can be transported to $M^{(n+2)+}=^{16}O$ to form $M^{(n+2)+}=^{18}O$, which can then react with PMS ^{16}O to form PMS $^{16}O^{18}O$. 239,246 Therefore, the detection of PMS $^{16}O^{18}O$ from mass spectrometry characterization provides critical evidence for $M^{(n+2)+}=O$.

Despite some literature discussion, two key questions remain: (1) what the actual oxidation state of the metal in metal-oxo species is and (2) how SAC differs from nanoparticle and dissolved ion in forming high-valent metal-oxo species. To answer the first question, some studies have employed ex situ XANES to examine the oxidation states of the metal after the reaction. 59,240 This is based on the unverified hypothesis that the high-valent metal-oxo species can stably remain on the catalyst surface after the reaction instead of being reduced back to lowvalent species to complete the redox cycle. However, high-valent species can (i) react with low-valent species to median-valent species (e.g., $Fe^{IV}O^{2+} + Fe^{2+} + 2H^+ \rightarrow 2Fe^{3+} + H_2O$, $k = 1.4 \times 10^5$ M^{-1} s⁻¹, pH = 1); 247,248 (ii) self-decay in H₂O (e.g., 4Fe^{IV}O²⁺ + $4H^+ \rightarrow 4Fe^{3+} + O_2 + 2H_2O, k = 0.1 \text{ s}^{-1});^{249} \text{ or (iii) react with}$ persulfate (e.g., $2Fe^{IV}O^{2+} + S_2O_8^{2-} \rightarrow 2Fe^{3+} + 2SO_4^{2-} + O_2, k = 1$ \times 10⁴ M⁻¹ s⁻¹). 250 In fact, ex situ methods likely measure the transformation products of high-valent species such as their protonated/hydrolyzed metal-oxo forms (e.g., FeN₄-OH/ FeN₄-O⁻) rather than the forms that participate in the actual persulfate reaction (e.g., $FeN_4=O$). Therefore, more accurate characterization should involve in situ XANES to identify, for example, the oxidation state increase during persulfate reaction. ^{241,251-253} High-valent metal-oxo references such as ferrates or oxo-iron porphyrin complexes should be used in such studies.25

The answer to the second question relates to persulfate decay pathways. Studies thus far provide some clues based on experimental observations but without firm mechanistic insights such as the impact of persulfate molecular alignment and detailed pathways toward $\equiv M^{(n+2)+} = O$ formation. For dissolved ions, the overall reaction between Fe²⁺ and PMS/PDS to generate Fe⁴⁺ is Fe²⁺ + HSO₅⁻ \rightarrow Fe^{IV}O²⁺ + SO₄²⁻ + H⁺, $k = 3 \times 10^4$ M⁻¹ s⁻¹;²⁵⁵ Fe²⁺ + S₂O₈²⁻ + H₂O \rightarrow Fe^{IV}O²⁺ + 2SO₄²⁻ + 2H⁺, $k = 2 \times 10^1$ M⁻¹ s⁻¹·²⁵⁰ A recent DFT analysis showed that homogeneous Co²⁺ and PMS interact via the type III configuration and generate high-valent Co⁴⁺=O₇ through the O_β-O_γ bond cleavage and the deprotonation. The mechanisms of SAC \equiv M⁽ⁿ⁺²⁾⁺=O formation may be similar as those in dissolved ions, *i.e.*, through the type III alignment configuration for SAC-PMS, with two-e⁻ transfer forming \equiv M⁽ⁿ⁺²⁾⁺=O_γ (Figure 6b). It was recently suggested that the SAC metal average oxidation state would determine whether the

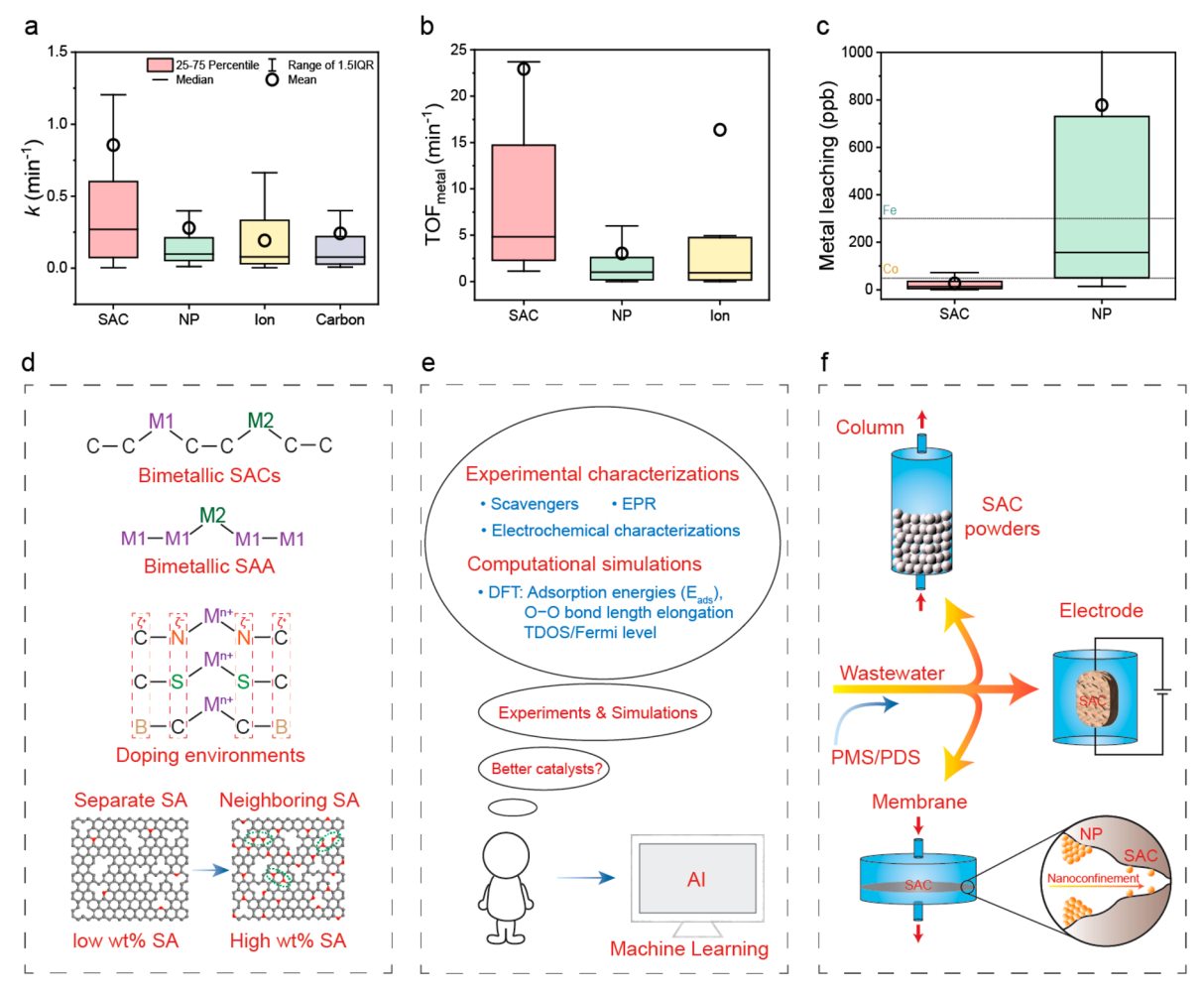


Figure 7. (a) First-order rate constant $k \, (\min^{-1})$ comparisons of SAC, nanoparticle (NP), dissolved ion, and carbon support for persulfate activation. Data used for the analysis are collected from more than 50 publications for each system. (b) TOF (\min^{-1}) comparisons of SAC, NP, and dissolved ion for persulfate activation. (c) Metal leaching (ppb) comparisons of SAC and NP during persulfate activation. Inset lines indicate the 50 ppb of Co and 300 ppb of Fe limitation in drinking water. (d) Material structural design and performance improvement. (e) Experiments and simulations: machine learning using AI simulations for rational design of persulfate catalysts. (f) Engineering consideration of real water treatment using SAC-persulfate technology.

radical pathway or high-valent species pathway is preferred in the Fe SAC-PMS system. The Fe²⁺–N₄ in the high-spin state (S = 2) tends to activate PMS to form $SO_4^{\bullet-}$ and OH radicals via an one-e transfer, while the Fe³⁺–N₄ (S = 5/2) is prone to Fe⁵⁺=O generation via two-e transfer. This points toward the possibility that the SAC's synthesis method (e.g., precursor choice, annealing or reduction conditions) may affect its mode of interaction with persulfate. Furthermore, it was suggested that, in the dissolved ion system, the persulfate activation to either high-valent species or radicals is also dependent on catalyst/persulfate relative amount and pH, which should also be evaluated in SAC-persulfate systems in the future.

Similar to the literature on $^{1}O_{2}$, there exist some controversies around the high-valent species mechanism. For example, in the Fe²⁺/PDS system, the rate constant of Fe²⁺ oxidation by PDS to form Fe^{IV}O²⁺ ($k = 2 \times 10^{1} \text{ M}^{-1} \text{ s}^{-1}$) is 3 orders of magnitude lower than that of Fe^{IV}O²⁺ reduction by PDS to form Fe³⁺ ($k = 1 \times 10^{4} \text{ M}^{-1} \text{ s}^{-1}$). So In addition, high-valent metal-oxo species are also known to exhibit much lower kinetics ($k = 10^{2} - 10^{4} \text{ M}^{-1} \text{ s}^{-1}$). Toward common organic pollutants than radicals ($k = 10^{6} - 10^{11} \text{ M}^{-1} \text{ s}^{-1}$), even slower than $^{1}O_{2}$ ($k = \sim 10^{2} - 10^{8} \text{ M}^{-1} \text{ s}^{-1}$). Other metal-oxo species such as $\equiv M^{(n+1)+} - OH/\equiv 10^{11} \text{ M}^{-1} \text{ s}^{-1}$.

 $M^{(n+1)+}$ $-O^-$ (formed by one-e⁻ transfer) and $\equiv M^{(n+2)+} \equiv O$ (formed by two-e⁻ transfer) are also critical intermediates in determining the mechanisms, which should be further characterized.

■ CHALLENGES AND RESEARCH DIRECTIONS

Our analysis on past studies suggest that many SACs achieve 3 to 4 times faster pollutant degradation kinetics compared to NP counterparts including metals and metal oxides (Figure 7a). Note that it is impossible to normalize the kinetics considering widely varying material properties and experimental conditions, and therefore, the comparison here should be taken only as a very rough estimate. The averaged kinetics among the papers we examined followed the order of: SACs > NPs > ions ≈ carbon substrates. The improved kinetics were achieved generally using much lower metal loading with SAC than other catalysts. Consequently, SACs exhibit significantly higher turnover frequencies (TOFs, min⁻¹) than NP counterparts and dissolved ions (Figure 7b). This collectively suggests that the original intent of combining the high atomic efficiency of homogeneous catalysts and the benefits of heterogeneous catalysts can be achieved. In addition, high TOF is beneficial to lower the cost of

materials especially for precious noble metals used for persulfate activation. We also note that the averaged metal leaching (ppb) from SACs is over 1 order of magnitude lower than nanoparticle counterparts (Figure 7c), even lower than the 50 ppb of Co and 300 ppb of Fe limits in drinking water. ^{91,258} Most benchmark nanoparticle catalysts (*e.g.*, Co NPs, Fe NPs, CoO_x, FeO_x, CoFeO_x, and MnO_x) for persulfate would lead to ppm levels of metal dissolution. The significantly improved stability of SACs, which likely results from a stronger interaction of SACs with the support via surface defects or N/O atom structure anchoring, is also crucial in lessening the impact of leached metal ions on water safety and ensuring long-term stability. With these initial promising findings, we below further discuss priority research areas to advance SACs for persulfate activation and ultimately toward practical application.

Mechanistic Investigation. We find that uncertainties still exist in consolidating different mechanisms in SAC-persulfate systems. For example, some key questions remain such as (i) whether the $\equiv M^{(n+1)+}$ can be readily reduced back to $\equiv M^{n+}$ to complete the redox cycle in the radical pathway; (ii) whether the $\equiv M-O$ intermediate on the SAC forms the 1O_2 intermediate; and (iii) how the higher oxidation state of the metal forms to drive the high-valent species pathway. Detailed studies into these key questions can help prove whether these activation mechanisms are valid or not. A better understanding of these mechanisms can help design catalysts that maximize the intended activation kinetics and selectivity.

We observe from our literature survey (Table S1) that more diverse activation mechanisms have been identified in SACpersulfate systems in comparison with conventional catalysts for which the radical pathway has been mostly considered as the dominant mechanism. We also notice more frequent claims on mediated electron transfer and high-valent species mechanisms with SACs. Although this trend still requires future confirmations by additional studies, we speculate that the reasons could be related to the fact that the overall loading percentages of SACs on the support are typically much lower than nanoparticles. Consequently, the electron transfer by substrate material might contribute more to the overall activation mechanism than intended. One notable example would be SACs on carbon support, wherein carbon plays a significant role in activating persulfate via electron transfer. In addition, SACs are likely to form the high-valent $\equiv M^{(n+2)+} = O$ structure considering their similarity to dissolved ions. We also believe that there is a vast uncertainty in how SACs function differently under different environmental conditions (e.g., pH, pollutant characteristics). Perhaps more importantly, SACs' properties may change significantly depending on their synthesis method, loading amount, and coordination environment. The experimental matrix considering all these factors appears extremely large, requiring further extensive and systematic research in understanding the role of SACs in persulfate activation.

Improved Material Design. The current designs of SACs for persulfate AOPs largely focus on varying types of TMs, supports (which are mainly constrained in carbon supports, Table S1), and persulfates. It is difficult to gauge how much the current material designs have achieved SACs' full potential for persulfate activation. Considering the experience that we have gained from designing nanoparticles for persulfate AOPs, there are likely several strategies to further improve the catalytic performance, and here we present three potentially impactful research directions (Figure 7d). First, similar to efforts in developing bimetallic NP catalysts, ^{259,260} SACs with more than

one metal can be explored. In spinel ferrites (MFe₂O₄, M = Cu, Co, Ni, etc.)^{261,262} or other weight combinations of bimetallic oxides, ^{263–265} the Fe site was shown to be able to offer synergistic effects including enhanced pollutant adsorption, ²⁶⁵ strong metal—metal magnetic interactions, ^{266–268} and facilitation of the redox cycle of the neighboring active metal (e.g., \equiv Fe²⁺ + \equiv Cu³⁺ \rightarrow \equiv Fe³⁺ + \equiv Cu^{2+,264} \equiv Fe²⁺ + \equiv Mn³⁺ \rightarrow \equiv Fe³⁺ + \equiv Mn²⁺²⁶⁵). Similarly, some recent studies have made early efforts in designing bimetallic SACs for PMS activations (e.g., Co–Fe, Bi–Fe), ^{172,269} yet the synergistic effects from two SACs require further investigation. The accurate control of material morphology would be a critical step, as to how two SACs are spatially distributed and how they collaborate toward synergistic effects (e.g., enhancing redox cycle). A material architecture may be expanded to SAC embedded or anchored on another metal NP/oxide support, forming a single atom alloy (SAA).

Second, we note that most SACs studied for persulfate activation were built upon the M-N-C structure, while SACs can be coordinated to other heteroatoms such as O, S, P, or B (e.g., S/N codoping for Co SAC, 270 N/B or N/P codoping for Cu SAC²⁷¹). The electronegativities of these elements follow the order: O ($\chi_{O} = 3.44$) > N ($\chi_{N} = 3.04$) > S ($\chi_{O} = 2.58$) > C (χ_{C} = 2.55) > P (χ_P = 2.19) > B (χ_B = 2.04). Consequently, these atoms can either donate or withdraw electrons from SACs, exerting either synergistic or antagonistic effects. 272-274 For example, O-, N-, S-, and B-doping were found to enhance persulfate activation by enhancing the persulfate ion adsorption via Lewis acid-base bonding, faster electron transfer, and/or a combination of these effects. 275-281 P-doping instead might scavenge SO₄ • or •OH, resulting in inhibition of the catalyst activity. ^{282,283} In all these cases, careful synthesis and characterization with changing dopant concentrations and controlled spatial distribution appear as prerequisites for further advancing the discussion on the kinetic benefits.

Finally, we would like to propose further focused research on strategies to drastically increase the weight loading of SACs. In fact, this would be the common goal for SAC research for all application fields, not just for persulfate activation. Some recent studies showed that when further increasing the SA wt % from ~1% (a typical loading of current SACs) to ~5%, SACs can form clusters without metal-metal bonding, which are often referred to as neighboring SACs or SAC ensembles.^{284,285} This SAC architecture partially resembles nanoparticles but still maintains the benefits of single atom dispersion such as high atomic efficiency and unique coordination environment. Further increasing the transition-metal SAC wt % to nearly 40% has recently been achieved using graphene quantum dots as the carbon support.²⁸⁶ In addition to more catalytic sites available for both persulfate activation and pollutant degradation, the evolution of different, potentially selective persulfate activation pathways is an additional expected benefit.

In Situ/Operando Characterizations. In situ techniques such as in situ XAS, ^{287,288} in situ Raman, ^{60,62,63} and in situ Mössbauer ^{289–291} can be instrumental in revealing SACs' chemical properties and electronic structure alteration during redox reactions, which are difficult to evaluate using ex situ techniques. ²⁸⁸ For example, in situ XAS was used to discover that the Fe–N–C catalyst structure changed from an initial nonplanar ferrous state to a planar ferric structure during the course of the ORR due to the axial bonding with O atom, significantly affecting the Fe SAC's ORR activity. ^{287,288} One can postulate that such a change might also be possible with

persulfate, since its O atom can similarly coordinate with Fe SACs. Future in situ findings on potential alteration of SACs with respect to their coordination environment during the course of persulfate activation and pollutant degradation can be helpful to explain persulfate activation mechanisms.²⁹² In situ XAS can also be helpful in verifying the existence of the ≡M-O structure, which is a critical, reactive, and possibly unstable intermediate that has been proposed to exist in all radical, ¹O₂, and high-valent pathways, as previously discussed. For example, the increase in the intensity of the \equiv M-N/O scattering in FT-EXAFS is a qualitative indication of the formation of \equiv M-OH or \equiv M-O structures. 287,288 Quantitively comparing the fitted coordination numbers (e.g., from CN = 4 of Fe $-N_4$ -C to CN = 5 of O-Fe-The oxidation state changes from in situ XANES can be directly used to confirm the formation of high-valent species (≡ $M^{(n+2)+}=0$).

Theoretical Simulations. Understanding how reactive species are generated and what factors affect their generation can help design better performing catalysts. The current theoretical simulations mainly report thermodynamic properties such as the adsorption energies $(E_{\rm ads})$, electron density, and charge accumulation surrounding the single atom site, the elongation of the O–O bond, the desorption energies $(E_{\rm des})$ of surface-bound radicals or anions, *etc.* (Figure 7e). To calculate all these parameters for each SAC on each different support, with possible variations in water quality parameters, using DFT is computationally too costly. Instead, rational design of persulfate catalysts based on machine learning and high-throughput simulations is likely a viable alternative. ²⁹³

Engineering Consideration. It would not be ideal to simply suspend SACs in a body of water, no matter which substrates they are anchored on, due to the requirement of mixing and subsequent separation from product water. Instead, SAC composite materials can be applied in a packed-bed column reactor, ²⁹⁴ as an electrode for electrocatalytic persulfate activation, ²⁹⁵ or onto membranes (Figure 7f). ^{91,296,297} The electrocatalytic approach appears appealing, since the atomic H* generated from noble metal cathodes (e.g., Pd + H $^+$ + e $^ \rightarrow$ Pd-H*) can serve as the catalyst to activate persulfate, ²⁹⁵ and the electrons from the cathode can reduce higher valent metal species to complete the metal redox cycle. 298 Anchoring onto membranes, whether electrified or not, also provides additional benefits of increased contact areas for surface reactions and the potential nanoconfinement effect of enhancing radical exposure in confined pores.²⁹⁹ In such a design, SACs provide a compelling advantage compared to their nanoparticle counterpart due to their size; i.e., for membranes with pores in the dimension of nanoscale, SACs become the only option to load catalysts inside the pores. For example, the loading of Co SAC inside a layered-graphene oxide membrane with effective pore sizes of 3-5 nm has recently been demonstrated. 91 Finally, while it is presumed that SACs are anchored more strongly onto substrates than nanoparticles, no comprehensive study has yet verified the long-term stability of SACs in real water treatment conditions. Perhaps a more important question is how resistant SACs are against aggregation/agglomeration (i.e., migration on the surface of the substrate and formation of clusters) especially under reactive conditions. Future research needs to consider these concerns that will determine whether efforts in advancing SACs will lead to fruition in practice.

ASSOCIATED CONTENT

5 Supporting Information

The Supporting Information is available free of charge at https://pubs.acs.org/doi/10.1021/acsestengg.2c00187.

Table summarizing recent SAC-persulfate studies including Fe, Co, Cu, Mn, Ag, Ni, and Ru with varied types of persulfates, supports, pollutants, mechanisms, and k values (PDF)

AUTHOR INFORMATION

Corresponding Author

Jae-Hong Kim − Department of Chemical and Environmental Engineering, Yale University, New Haven, Connecticut 06511, United States; orcid.org/0000-0003-2224-3516; Phone: +1-203-432-4386; Email: jaehong.kim@yale.edu; Fax: +1-203-432-4387

Author

Xuanhao Wu — Department of Chemical and Environmental Engineering, Yale University, New Haven, Connecticut 06511, United States; Orcid.org/0000-0001-6177-6089

Complete contact information is available at: https://pubs.acs.org/10.1021/acsestengg.2c00187

Notes

The authors declare no competing financial interest.

ACKNOWLEDGMENTS

This study was partly supported by the National Science Foundation (NSF) Grant #1955793 under the Division of Chemical, Bioengineering, Environmental, and Transport Systems (CBET).

REFERENCES

- (1) Glaze, W. H.; Kang, J.-W.; Chapin, D. H. The chemistry of water treatment processes involving ozone, hydrogen peroxide and ultraviolet radiation. *Ozone Sci. Eng.* **1987**, *9* (4), 335.
- (2) Andreozzi, R.; Caprio, V.; Insola, A.; Marotta, R. Advanced oxidation processes (AOP) for water purification and recovery. *Catal. Today* **1999**, 53 (1), 51–59.
- (3) Haji, S.; Benstaali, B.; Al-Bastaki, N. Degradation of methyl orange by UV/H_2O_2 advanced oxidation process. *Chem. Eng. J.* **2011**, *168* (1), 134–139.
- (4) Jin, J.; El-Din, M. G.; Bolton, J. R. Assessment of the UV/chlorine process as an advanced oxidation process. *Water Res.* **2011**, *45* (4), 1890–1896.
- (5) Lee, J.; Von Gunten, U.; Kim, J.-H. Persulfate-based advanced oxidation: critical assessment of opportunities and roadblocks. *Environ. Sci. Technol.* **2020**, *54* (6), 3064–3081.
- (6) Wu, S.; Shen, L.; Lin, Y.; Yin, K.; Yang, C. Sulfite-based advanced oxidation and reduction processes for water treatment. *Chem. Eng. J.* **2021**, 414, 128872.
- (7) Sun, P.; Meng, T.; Wang, Z.; Zhang, R.; Yao, H.; Yang, Y.; Zhao, L. Degradation of organic micropollutants in UV/NH₂Cl advanced oxidation process. *Environ. Sci. Technol.* **2019**, *53* (15), 9024–9033.
- (8) Kim, J.; Zhang, T.; Liu, W.; Du, P.; Dobson, J. T.; Huang, C.-H. Advanced oxidation process with peracetic acid and Fe (II) for contaminant degradation. *Environ. Sci. Technol.* **2019**, 53 (22), 13312–13322
- (9) Mokudai, T.; Nakamura, K.; Kanno, T.; Niwano, Y. Presence of hydrogen peroxide, a source of hydroxyl radicals, in acid electrolyzed water. *PLoS One* **2012**, *7* (9), e46392.
- (10) Sies, H. Strategies of antioxidant defense. Eur. J. Biochem. 1993, 215 (2), 213–219.

- (11) Ghanbari, F.; Moradi, M. Application of peroxymonosulfate and its activation methods for degradation of environmental organic pollutants. *Chem. Eng. J.* **2017**, 310, 41–62.
- (12) Oh, W.-D.; Dong, Z.; Lim, T.-T. Generation of sulfate radical through heterogeneous catalysis for organic contaminants removal: current development, challenges and prospects. *Appl. Catal. B Environ.* **2016**, *194*, 169–201.
- (13) Wang, J.; Wang, S. Activation of persulfate (PS) and peroxymonosulfate (PMS) and application for the degradation of emerging contaminants. *Chem. Eng. J.* **2018**, 334, 1502–1517.
- (14) Anipsitakis, G. P.; Dionysiou, D. D. Radical generation by the interaction of transition metals with common oxidants. *Environ. Sci. Technol.* **2004**, 38 (13), 3705–3712.
- (15) Luo, C.; Ma, J.; Jiang, J.; Liu, Y.; Song, Y.; Yang, Y.; Guan, Y.; Wu, D. Simulation and comparative study on the oxidation kinetics of atrazine by UV/H_2O_2 , UV/HSO_5^- and $UV/S_2O_8^{2-}$. Water Res. **2015**, 80, 99–108.
- (16) Fang, G.-D.; Dionysiou, D. D.; Wang, Y.; Al-Abed, S. R.; Zhou, D.-M. Sulfate radical-based degradation of polychlorinated biphenyls: effects of chloride ion and reaction kinetics. *J. Hazard. Mater.* **2012**, 227, 394–401.
- (17) Song, Y.; Fang, G.; Zhu, C.; Zhu, F.; Wu, S.; Chen, N.; Wu, T.; Wang, Y.; Gao, J.; Zhou, D. Zero-valent iron activated persulfate remediation of polycyclic aromatic hydrocarbon-contaminated soils: an in situ pilot-scale study. *Chem. Eng. J.* **2019**, *355*, 65–75.
- (18) Li, Y.-T.; Zhang, J.-J.; Li, Y.-H.; Chen, J.-L.; Du, W.-Y. Treatment of soil contaminated with petroleum hydrocarbons using activated persulfate oxidation, ultrasound, and heat: A kinetic and thermodynamic study. *Chem. Eng. J.* **2022**, *428*, 131336.
- (19) Chen, G.; Yu, Y.; Liang, L.; Duan, X.; Li, R.; Lu, X.; Yan, B.; Li, N.; Wang, S. Remediation of antibiotic wastewater by coupled photocatalytic and persulfate oxidation system: A critical review. *J. Hazard. Mater.* **2021**, 408, 124461.
- (20) Zhang, P.; Song, D.; Hao, Y.; Shang, X.; Wang, C.; Tang, J.; Sun, H. Sulfidated zero valent iron as a persulfate activator for oxidizing organophosphorus pesticides (OPPs) in aqueous solution and aged contaminated soil columns. *Chemosphere* **2021**, *281*, 130760.
- (21) Ding, S.; Wan, J.; Ma, Y.; Wang, Y.; Li, X.; Sun, J.; Pu, M. Targeted degradation of dimethyl phthalate by activating persulfate using molecularly imprinted Fe-MOF-74. *Chemosphere* **2021**, 270, 128620.
- (22) Wu, J.; Wang, B.; Cagnetta, G.; Huang, J.; Wang, Y.; Deng, S.; Yu, G. Nanoscale zero valent iron-activated persulfate coupled with Fenton oxidation process for typical pharmaceuticals and personal care products degradation. *Sep. Purif. Technol.* **2020**, 239, 116534.
- (23) Xiao, S.; Cheng, M.; Zhong, H.; Liu, Z.; Liu, Y.; Yang, X.; Liang, Q. Iron-mediated activation of persulfate and peroxymonosulfate in both homogeneous and heterogeneous ways: a review. *Chem. Eng. J.* **2020**, 384, 123265.
- (24) Anipsitakis, G. P.; Dionysiou, D. D.; Gonzalez, M. A. Cobalt-mediated activation of peroxymonosulfate and sulfate radical attack on phenolic compounds. Implications of chloride ions. *Environ. Sci. Technol.* **2006**, *40* (3), 1000–1007.
- (25) Lee, H.-J.; Kim, H.-E.; Kim, M. S.; de Lannoy, C.-F.; Lee, C. Inactivation of bacterial planktonic cells and biofilms by Cu(II)-activated peroxymonosulfate in the presence of chloride ion. *Chem. Eng. J.* 2020, 380, 122468.
- (26) Dong, H.; Qiang, Z.; Hu, J.; Sans, C. Accelerated degradation of iopamidol in iron activated persulfate systems: roles of complexing agents. *Chem. Eng. J.* **2017**, *316*, 288–295.
- (27) Wu, S.; Hu, Y. H. A comprehensive review on catalysts for electrocatalytic and photoelectrocatalytic degradation of antibiotics. *Chem. Eng. J.* **2021**, *409*, 127739.
- (28) Ahn, Y.-Y.; Bae, H.; Kim, H.-I.; Kim, S.-H.; Kim, J.-H.; Lee, S.-G.; Lee, J. Surface-loaded metal nanoparticles for peroxymonosulfate activation: Efficiency and mechanism reconnaissance. *Appl. Catal. B Environ.* **2019**, 241, 561–569.
- (29) Xiao, R.; Luo, Z.; Wei, Z.; Luo, S.; Spinney, R.; Yang, W.; Dionysiou, D. D. Activation of peroxymonosulfate/persulfate by

- nanomaterials for sulfate radical-based advanced oxidation technologies. Current Opin. Chem. Eng. 2018, 19, 51-58.
- (30) Wang, A.; Li, J.; Zhang, T. Heterogeneous single-atom catalysis. *Nat. Rev. Chem.* **2018**, 2 (6), 65–81.
- (31) Yang, X.-F.; Wang, A.; Qiao, B.; Li, J.; Liu, J.; Zhang, T. Single-atom catalysts: a new frontier in heterogeneous catalysis. *Acc. Chem. Res.* **2013**, *46* (8), 1740–1748.
- (32) Qiao, B.; Wang, A.; Yang, X.; Allard, L. F.; Jiang, Z.; Cui, Y.; Liu, J.; Li, J.; Zhang, T. J. N. c. Single-atom catalysis of CO oxidation using Pt₁/FeO_x. *Nat. Chem.* **2011**, *3* (8), 634–641.
- (33) Lang, R.; Xi, W.; Liu, J.-C.; Cui, Y.-T.; Li, T.; Lee, A. F.; Chen, F.; Chen, Y.; Li, L.; Li, L. Non defect-stabilized thermally stable single-atom catalyst. *Nat. Commun.* **2019**, *10*, 234.
- (34) Huang, B.; Wu, Z.; Zhou, H.; Li, J.; Zhou, C.; Xiong, Z.; Pan, Z.; Yao, G.; Lai, B. Recent advances in single-atom catalysts for advanced oxidation processes in water purification. *J. Hazard. Mater.* **2021**, *412*, 125253
- (35) Podyacheva, O. Y.; Bulushev, D. A.; Suboch, A. N.; Svintsitskiy, D. A.; Lisitsyn, A. S.; Modin, E.; Chuvilin, A.; Gerasimov, E. Y.; Sobolev, V. I.; Parmon, V. N. Highly Stable Single-Atom Catalyst with Ionic Pd Active Sites Supported on N-Doped Carbon Nanotubes for Formic Acid Decomposition. *ChemSusChem* **2018**, *11* (21), 3724–3727.
- (36) Jones, J.; Xiong, H.; DeLaRiva, A. T.; Peterson, E. J.; Pham, H.; Challa, S. R.; Qi, G.; Oh, S.; Wiebenga, M. H.; Hernández, X. I. P. Thermally stable single-atom platinum-on-ceria catalysts via atom trapping. *Science* **2016**, 353 (6295), 150–154.
- (37) Song, P.; Luo, M.; Liu, X.; Xing, W.; Xu, W.; Jiang, Z.; Gu, L. Zn single atom catalyst for highly efficient oxygen reduction reaction. *Adv. Fun. Mater.* **2017**, *27* (28), 1700802.
- (38) Cheng, N.; Stambula, S.; Wang, D.; Banis, M. N.; Liu, J.; Riese, A.; Xiao, B.; Li, R.; Sham, T.-K.; Liu, L.-M. Platinum single-atom and cluster catalysis of the hydrogen evolution reaction. *Nat. Commun.* **2016**, *7*, 13638.
- (39) Zheng, T.; Jiang, K.; Ta, N.; Hu, Y.; Zeng, J.; Liu, J.; Wang, H. Large-scale and highly selective CO₂ electrocatalytic reduction on nickel single-atom catalyst. *Joule* **2019**, 3 (1), 265–278.
- (40) Chu, C.; Yang, J.; Zhou, X.; Huang, D.; Qi, H.; Weon, S.; Li, J.; Elimelech, M.; Wang, A.; Kim, J.-H. Cobalt single atoms on tetrapyridomacrocyclic support for efficient peroxymonosulfate activation. *Environ. Sci. Technol.* **2021**, *55* (2), 1242–1250.
- (41) Huang, D.; de Vera, G. A.; Chu, C.; Zhu, Q.; Stavitski, E.; Mao, J.; Xin, H.; Spies, J. A.; Schmuttenmaer, C. A.; Niu, J.; Haller, G. L.; Kim, J.-H. Single-atom Pt catalyst for effective C–F bond activation via hydrodefluorination. *ACS Catal.* **2018**, 8 (10), 9353–9358.
- (42) Li, N.; Song, X.; Wang, L.; Geng, X.; Wang, H.; Tang, H.; Bian, Z. Single-atom cobalt catalysts for electrocatalytic hydrodechlorination and oxygen reduction reaction for the degradation of chlorinated organic compounds. ACS Appl. Mater. Interfaces 2020, 12 (21), 24019—24029
- (43) Li, P.; Jin, Z.; Fang, Z.; Yu, G. A single-site iron catalyst with preoccupied active centers that achieves selective ammonia electrosynthesis from nitrate. *Ener. Environ. Sci.* **2021**, *14* (6), 3522–3531.
- (44) Wu, Z.-Y.; Karamad, M.; Yong, X.; Huang, Q.; Cullen, D. A.; Zhu, P.; Xia, C.; Xiao, Q.; Shakouri, M.; Chen, F.-Y. Electrochemical ammonia synthesis via nitrate reduction on Fe single atom catalyst. *Nat. Commun.* **2021**, *12*, 2870.
- (45) An, S.; Zhang, G.; Wang, T.; Zhang, W.; Li, K.; Song, C.; Miller, J. T.; Miao, S.; Wang, J.; Guo, X. High-density ultra-small clusters and single-atom Fe sites embedded in graphitic carbon nitride (g-C₃N₄) for highly efficient catalytic advanced oxidation processes. *ACS Nano* **2018**, 12 (9), 9441–9450.
- (46) Li, X.; Huang, X.; Xi, S.; Miao, S.; Ding, J.; Cai, W.; Liu, S.; Yang, X.; Yang, H.; Gao, J. Single cobalt atoms anchored on porous N-doped graphene with dual reaction sites for efficient Fenton-like catalysis. *J. Am. Chem. Soc.* **2018**, *140* (39), 12469–12475.
- (47) Wang, Y.; Zhao, X.; Cao, D.; Wang, Y.; Zhu, Y. Peroxymonosulfate enhanced visible light photocatalytic degradation bisphenol A by single-atom dispersed Ag mesoporous g-C₃N₄ hybrid. *Appl. Catal. B Environ.* **2017**, *211*, 79–88.

- (48) Xu, J.; Zheng, X.; Feng, Z.; Lu, Z.; Zhang, Z.; Huang, W.; Li, Y.; Vuckovic, D.; Li, Y.; Dai, S.; Chen, G.; Wang, K.; Wang, H.; Chen, J. K.; Mitch, W.; Cui, Y. Organic wastewater treatment by a single-atom catalyst and electrolytically produced $\rm H_2O_2$. Nat. Sustain. 2021, 4 (3), 233–241.
- (49) Han, B.; Luo, Y.; Lin, Y.; Weng, B.; Xia, D.; Zhou, Y.; Guan, C.; Wang, Z.; Wei, X.; Jiang, J. Microenvironment engineering of single-atom catalysts for persulfate-based advanced oxidation processes. *Chem. Eng. J.* 2022, 447, 137551.
- (50) Shang, Y.; Xu, X.; Gao, B.; Wang, S.; Duan, X. Single-atom catalysis in advanced oxidation processes for environmental remediation. *Chem. Soc. Rev.* **2021**, *50* (8), 5281–5322.
- (51) Wang, X.; Yunping, T.; Fang, G. Advances of single-atom catalysts for applications in persulfate-based advanced oxidation technologies. *Current Opin. Chem. Eng.* **2021**, *34*, 100757.
- (52) Li, J.; Zhao, S.; Yang, S.-Z.; Wang, S.; Sun, H.; Johannessen, B.; Liu, S. Atomically dispersed cobalt on graphitic carbon nitride as a robust catalyst for selective oxidation of ethylbenzene by peroxymonosulfate. *J. Mater. Chem. A* **2021**, *9* (5), 3029–3035.
- (53) Li, J.; Zhao, S.; Zhang, L.; Jiang, S. P.; Yang, S. Z.; Wang, S.; Sun, H.; Johannessen, B.; Liu, S. Cobalt Single Atoms Embedded in Nitrogen-Doped Graphene for Selective Oxidation of Benzyl Alcohol by Activated Peroxymonosulfate. *Small* **2021**, *17* (16), 2004579.
- (54) Mi, X.; Wang, P.; Xu, S.; Su, L.; Zhong, H.; Wang, H.; Li, Y.; Zhan, S. Almost 100% peroxymonosulfate conversion to singlet oxygen on single-atom CoN₂₊₂ sites. *Angew. Chem.* **2021**, *133* (9), 4638–4643.
- (55) Qi, Y.; Li, J.; Zhang, Y.; Cao, Q.; Si, Y.; Wu, Z.; Akram, M.; Xu, X. Novel lignin-based single atom catalysts as peroxymonosulfate activator for pollutants degradation: role of single cobalt and electron transfer pathway. *Appl. Catal. B Environ.* **2021**, *286*, 119910.
- (56) Xu, H.; Jiang, N.; Wang, D.; Wang, L.; Song, Y.; Chen, Z.; Ma, J.; Zhang, T. Improving PMS oxidation of organic pollutants by single cobalt atom catalyst through hybrid radical and non-radical pathways. *Appl. Catal. B Environ.* **2020**, 263, 118350.
- (57) Gao, Y.; Zhu, Y.; Li, T.; Chen, Z.; Jiang, Q.; Zhao, Z.; Liang, X.; Hu, C. Unraveling the High-Activity Origin of Single-Atom Iron Catalysts for Organic Pollutant Oxidation via Peroxymonosulfate Activation. *Environ. Sci. Technol.* **2021**, *55* (12), 8318–8328.
- (58) Miao, W.; Liu, Y.; Wang, D.; Du, N.; Ye, Z.; Hou, Y.; Mao, S.; Ostrikov, K. K. The role of Fe-N_x single-atom catalytic sites in peroxymonosulfate activation: Formation of surface-activated complex and non-radical pathways. *Chem. Eng. J.* **2021**, *423*, 130250.
- (59) Qian, K.; Chen, H.; Li, W.; Ao, Z.; Wu, Y.-n.; Guan, X. Single-Atom Fe Catalyst Outperforms Its Homogeneous Counterpart for Activating Peroxymonosulfate to Achieve Effective Degradation of Organic Contaminants. *Environ. Sci. Technol.* **2021**, *55* (10), 7034–7043.
- (60) Yang, T.; Fan, S.; Li, Y.; Zhou, Q. Fe-N/C single-atom catalysts with high density of Fe-Nx sites toward peroxymonosulfate activation for high-efficient oxidation of bisphenol A: Electron-transfer mechanism. *Chem. Eng. J.* **2021**, *419*, 129590.
- (61) Chen, F.; Wu, X.-L.; Yang, L.; Chen, C.; Lin, H.; Chen, J. Efficient degradation and mineralization of antibiotics via heterogeneous activation of peroxymonosulfate by using graphene supported single-atom Cu catalyst. *Chem. Eng. J.* **2020**, 394, 124904.
- (62) Pan, J.; Gao, B.; Duan, P.; Guo, K.; Akram, M.; Xu, X.; Yue, Q.; Gao, Y. Improving peroxymonosulfate activation by copper ion-saturated adsorbent-based single atom catalysts for the degradation of organic contaminants: electron-transfer mechanism and the key role of Cu single atoms. *J. Mater. Chem. A* **2021**, *9* (19), 11604–11613.
- (63) Miao, J.; Zhu, Y.; Lang, J.; Zhang, J.; Cheng, S.; Zhou, B.; Zhang, L.; Alvarez, P. J.; Long, M. Spin-State-Dependent Peroxymonosulfate Activation of Single-Atom M—N Moieties via a Radical-Free Pathway. *ACS Catal.* **2021**, *11*, 9569–9577.
- (64) Wang, Y.; Zhao, X.; Cao, D.; Wang, Y.; Zhu, Y. Peroxymonosulfate enhanced visible light photocatalytic degradation bisphenol A by single-atom dispersed Ag mesoporous g-C₃N₄ hybrid. *Applied Catalysis B: Environmental* **2017**, 211, 79–88.

- (65) Yan, Y.; Yang, Q.; Shang, Q.; Ai, J.; Yang, X.; Wang, D.; Liao, G. Ru doped graphitic carbon nitride mediated peroxymonosulfate activation for diclofenac degradation via singlet oxygen. *Chem. Eng. J.* **2021**, *430* (4), 133174.
- (66) Duan, X.; Sun, H.; Tade, M.; Wang, S. Metal-free activation of persulfate by cubic mesoporous carbons for catalytic oxidation via radical and nonradical processes. *Catal. Today* **2018**, 307, 140–146.
- (67) Tang, L.; Liu, Y.; Wang, J.; Zeng, G.; Deng, Y.; Dong, H.; Feng, H.; Wang, J.; Peng, B. Enhanced activation process of persulfate by mesoporous carbon for degradation of aqueous organic pollutants: Electron transfer mechanism. *Appl. Catal. B Environ.* **2018**, 231, 1–10.
- (68) Zhou, Z.; Li, M.; Kuai, C.; Zhang, Y.; Smith, V. F.; Lin, F.; Aiello, A.; Durkin, D. P.; Chen, H.; Shuai, D. Fe-based Single-Atom Catalysis for Oxidizing Contaminants of Emerging Concern by Activating Peroxides. *J. Hazard. Mater.* **2021**, *418*, 126294.
- (69) Chen, L.; Xing, K.; Shentu, Q.; Huang, Y.; Lv, W.; Yao, Y. Well-dispersed iron and nitrogen co-doped hollow carbon microsphere anchoring by $g\text{-}C_3N_4$ for efficient peroxymonosulfate activation. *Chemosphere* **2021**, 280, 130911.
- (70) Miao, W.; Liu, Y.; Wang, D.; Du, N.; Ye, Z.; Hou, Y.; Mao, S.; Ostrikov, K. K. The role of Fe-Nx single-atom catalytic sites in peroxymonosulfate activation: formation of surface-activated complex and non-radical pathways. *Chemical Engineering Journal* **2021**, 423, 130250.
- (71) Song, H.; Du, R.; Wang, Y.; Zu, D.; Zhou, R.; Cai, Y.; Wang, F.; Li, Z.; Shen, Y.; Li, C. Anchoring single atom cobalt on two-dimensional MXene for activation of peroxymonosulfate. *Appl. Catal. B Environ.* **2021**, 286, 119898.
- (72) Wang, Z.; Yang, H.; Liu, R.; Xie, S.; Liu, Y.; Dai, H.; Huang, H.; Deng, J. Probing toluene catalytic removal mechanism over supported Pt nano-and single-atom-catalyst. *J. Hazard. Mater.* **2020**, 392, 122258.
- (73) Mi, X.; Wang, P.; Xu, S.; Su, L.; Zhong, H.; Wang, H.; Li, Y.; Zhan, S. Almost 100% peroxymonosulfate conversion to singlet oxygen on single-atom CoN₂₊₂ sites. *Angew. Chem.* **2021**, 133 (9), 4638–4643.
- (74) Yao, Y.; Yin, H.; Gao, M.; Hu, Y.; Hu, H.; Yu, M.; Wang, S. Electronic structure modulation of covalent organic frameworks by single-atom Fe doping for enhanced oxidation of aqueous contaminants. *Chem. Eng. Sci.* 2019, 209, 115211.
- (75) Long, Y.; Huang, Y.; Wu, H.; Shi, X.; Xiao, L. Peroxymonosulfate activation for pollutants degradation by Fe-N-codoped carbonaceous catalyst: Structure-dependent performance and mechanism insight. *Chem. Eng. J.* **2019**, 369, 542–552.
- (76) Zhang, H.; Lyu, L.; Fang, Q.; Hu, C.; Zhan, S.; Li, T. Cation— π structure inducing efficient peroxymonosulfate activation for pollutant degradation over atomically dispersed cobalt bonding graphene-like nanospheres. *Appl. Catal. B Environ.* **2021**, 286, 119912.
- (77) Wang, T.; Zhou, J.; Wang, W.; Zhu, Y.; Niu, J. Ag-single atoms modified S_1 . $_{66}$ - $N_{1.\ 91}$ / TiO_2 -x for photocatalytic activation of peroxymonosulfate for bisphenol A degradation. *Chin. Chem. Lett.* **2022**, 33 (4), 2121–2124.
- (78) Xu, L.; Liu, L. Piezo-photocatalytic Fuel Cell with Atomic Fe@ MoS₂ on CFC Helical Electrode Has Enhanced Peroxymonosulfate Activation, Pollutant Degradation and Power Generation. *Appl. Catal. B Environ.* **2022**, *304*, 120953.
- (79) Lang, R.; Du, X.; Huang, Y.; Jiang, X.; Zhang, Q.; Guo, Y.; Liu, K.; Qiao, B.; Wang, A.; Zhang, T. Single-atom catalysts based on the metal—oxide interaction. *Chem. Rev.* **2020**, *120* (21), 11986—12043.
- (80) Hannagan, R. T.; Giannakakis, G.; Flytzani-Stephanopoulos, M.; Sykes, E. C. H. Single-atom alloy catalysis. *Chem. Rev.* **2020**, *120* (21), 12044–12088.
- (81) Weon, S.; Huang, D.; Rigby, K.; Chu, C.; Wu, X.; Kim, J.-H. Environmental materials beyond and below the nanoscale: Single-atom catalysts. *ACS EST Engg.* **2021**, *1* (2), 157–172.
- (82) Zhang, H.; Liu, G.; Shi, L.; Ye, J. Single-atom catalysts: emerging multifunctional materials in heterogeneous catalysis. *Adv. Ener. Mater.* **2018**, *8* (1), 1701343.
- (83) Rivera-Cárcamo, C.; Serp, P. Single atom catalysts on carbon-based materials. *ChemCatChem.* **2018**, *10* (22), 5058–5091.

- (84) Singh, B.; Gawande, M. B.; Kute, A. D.; Varma, R. S.; Fornasiero, P.; McNeice, P.; Jagadeesh, R. V.; Beller, M.; Zbořil, R. Single-atom (iron-based) catalysts: synthesis and applications. *Chem. Rev.* **2021**, *121* (21), 13620–13697.
- (85) Shang, Y.; Duan, X.; Wang, S.; Yue, Q.; Gao, B.; Xu, X. Carbonbased single atom catalyst: Synthesis, characterization, DFT calculations. *Chin. Chem. Lett.* **2022**, *33* (2), 663–673.
- (86) Cheng, N.; Zhang, L.; Doyle-Davis, K.; Sun, X. Single-atom catalysts: from design to application. *Electrochem. Ener. Rev.* **2019**, 2 (4), 539–573.
- (87) Chen, Y.; Ji, S.; Chen, C.; Peng, Q.; Wang, D.; Li, Y. Single-atom catalysts: synthetic strategies and electrochemical applications. *Joule* **2018**, 2 (7), 1242–1264.
- (88) Zhang, L.; Ren, Y.; Liu, W.; Wang, A.; Zhang, T. Single-atom catalyst: a rising star for green synthesis of fine chemicals. *Nat. Sci. Rev.* **2018**, *5* (5), 653–672.
- (89) Ji, S.; Chen, Y.; Wang, X.; Zhang, Z.; Wang, D.; Li, Y. Chemical synthesis of single atomic site catalysts. *Chem. Rev.* **2020**, *120* (21), 11900–11955.
- (90) Wang, J.; Li, Z.; Wu, Y.; Li, Y. Fabrication of single-atom catalysts with precise structure and high metal loading. *Adv. Mater.* **2018**, *30* (48), 1801649.
- (91) Wu, X.; Rigby, K.; Huang, D.; Hedtke, T.; Wang, X.; Chung, M. W.; Weon, S.; Stavitski, E.; Kim, J.-H. Single-Atom Cobalt Incorporated in a 2D Graphene Oxide Membrane for Catalytic Pollutant Degradation. *Environ. Sci. Technol.* **2022**, *56* (2), 1341–1351.
- (92) Zhang, H.; Kawashima, K.; Okumura, M.; Toshima, N. Colloidal Au single-atom catalysts embedded on Pd nanoclusters. *J. Mater. Chem. A* **2014**, 2 (33), 13498–13508.
- (93) Ge, X.; Zhou, P.; Zhang, Q.; Xia, Z.; Chen, S.; Gao, P.; Zhang, Z.; Gu, L.; Guo, S. Palladium single atoms on TiO₂ as a photocatalytic sensing platform for analyzing the organophosphorus pesticide chlorpyrifos. *Angew. Chem.* **2020**, *132* (1), 238–242.
- (94) Liu, P.; Zhao, Y.; Qin, R.; Mo, S.; Chen, G.; Gu, L.; Chevrier, D. M.; Zhang, P.; Guo, Q.; Zang, D. Photochemical route for synthesizing atomically dispersed palladium catalysts. *Science* **2016**, *352* (6287), 797–800.
- (95) Gao, C.; Chen, S.; Wang, Y.; Wang, J.; Zheng, X.; Zhu, J.; Song, L.; Zhang, W.; Xiong, Y. Heterogeneous single-atom catalyst for visible-light-driven high-turnover CO₂ reduction: the role of electron transfer. *Adv. Mater.* **2018**, *30* (13), 1704624.
- (96) Chen, Y.; Ji, S.; Sun, W.; Chen, W.; Dong, J.; Wen, J.; Zhang, J.; Li, Z.; Zheng, L.; Chen, C. Discovering partially charged single-atom Pt for enhanced anti-Markovnikov alkene hydrosilylation. *J. Am. Chem. Soc.* 2018, 140 (24), 7407–7410.
- (97) Hu, J.-C.; Gui, M.-X.; Xia, W.; Wu, J.; Zhou, Y.-N.; Feng, N.; Xiao, J.; Liu, H.; Tung, C.-H.; Wu, L.-Z. Facile formation of CoN₄ active sites onto a SiO₂ support to achieve robust CO₂ and proton reduction in a noble-metal-free photocatalytic system. *J. Mater. Chem. A* **2019**, 7 (17), 10475–10482.
- (98) Huang, D.; He, N.; Zhu, Q.; Chu, C.; Weon, S.; Rigby, K.; Zhou, X.; Xu, L.; Niu, J.; Stavitski, E. Conflicting Roles of Coordination Number on Catalytic Performance of Single-Atom Pt Catalysts. *ACS Catal.* **2021**, *11* (9), 5586–5592.
- (99) Choi, C. H.; Kim, M.; Kwon, H. C.; Cho, S. J.; Yun, S.; Kim, H.-T.; Mayrhofer, K. J.; Kim, H.; Choi, M. Tuning selectivity of electrochemical reactions by atomically dispersed platinum catalyst. *Nat. Commun.* **2016**, *7*, 10922.
- (100) Lim, T.; Kim, J. H.; Kim, J.; Baek, D. S.; Shin, T. J.; Jeong, H. Y.; Lee, K.-S.; Exner, K. S.; Joo, S. H. General Efficacy of Atomically Dispersed Pt Catalysts for the Chlorine Evolution Reaction: Potential-Dependent Switching of the Kinetics and Mechanism. *ACS Catal.* **2021**, *11* (19), 12232–12246.
- (101) Chu, X.; Qu, Y.; Zada, A.; Bai, L.; Li, Z.; Yang, F.; Zhao, L.; Zhang, G.; Sun, X.; Yang, Z. D. Ultrathin Phosphate-Modulated Co Phthalocyanine/g-C₃N₄ Heterojunction Photocatalysts with Single Co-N₄(II) Sites for Efficient O₂ Activation. *Adv. Sci.* **2020**, 7 (16), 2001543.

- (102) Li, J.; Chen, S.; Yang, N.; Deng, M.; Ibraheem, S.; Deng, J.; Li, J.; Li, L.; Wei, Z. Ultrahigh-loading zinc single-atom catalyst for highly efficient oxygen reduction in both acidic and alkaline media. *Angew. Chem.* **2019**, 58 (21), 7035–7039.
- (103) Lim, T.; Jung, G. Y.; Kim, J. H.; Park, S. O.; Park, J.; Kim, Y.-T.; Kang, S. J.; Jeong, H. Y.; Kwak, S. K.; Joo, S. H. Atomically dispersed Pt–N₄ sites as efficient and selective electrocatalysts for the chlorine evolution reaction. *Nat. Commun.* **2020**, *11*, 412.
- (104) Yang, H.; Shang, L.; Zhang, Q.; Shi, R.; Waterhouse, G. I.; Gu, L.; Zhang, T. A universal ligand mediated method for large scale synthesis of transition metal single atom catalysts. *Nat. Commun.* **2019**, 10, 4585.
- (105) Han, A.; Wang, B.; Kumar, A.; Qin, Y.; Jin, J.; Wang, X.; Yang, C.; Dong, B.; Jia, Y.; Liu, J. Recent advances for MOF-derived carbon-supported single-atom catalysts. *Small Methods* **2019**, *3* (9), 1800471.
- (106) Jiao, L.; Jiang, H.-L. Metal-organic-framework-based single-atom catalysts for energy applications. *Chem.* **2019**, *5* (4), 786–804.
- (107) Jiang, R.; Li, L.; Sheng, T.; Hu, G.; Chen, Y.; Wang, L. Edge-site engineering of atomically dispersed Fe–N₄ by selective C–N bond cleavage for enhanced oxygen reduction reaction activities. *J. Am. Chem. Soc.* **2018**, *140* (37), 11594–11598.
- (108) Yang, Y.; Mao, K.; Gao, S.; Huang, H.; Xia, G.; Lin, Z.; Jiang, P.; Wang, C.; Wang, H.; Chen, Q. O-, N-atoms-coordinated Mn cofactors within a graphene framework as bioinspired oxygen reduction reaction electrocatalysts. *Adv. Mater.* **2018**, *30* (28), 1801732.
- (109) Fan, L.; Liu, P. F.; Yan, X.; Gu, L.; Yang, Z. Z.; Yang, H. G.; Qiu, S.; Yao, X. Atomically isolated nickel species anchored on graphitized carbon for efficient hydrogen evolution electrocatalysis. *Nat. Commun.* **2016**, *7*, 10667.
- (110) Zhang, L.; Jia, Y.; Liu, H.; Zhuang, L.; Yan, X.; Lang, C.; Wang, X.; Yang, D.; Huang, K.; Feng, S. Charge polarization from atomic metals on adjacent graphitic layers for enhancing the hydrogen evolution reaction. *Angew. Chem.* **2019**, *131* (28), 9504–9508.
- (111) Moliner, M.; Gabay, J. E.; Kliewer, C. E.; Carr, R. T.; Guzman, J.; Casty, G. L.; Serna, P.; Corma, A. Reversible transformation of Pt nanoparticles into single atoms inside high-silica chabazite zeolite. *J. Am. Chem. Soc.* **2016**, *138* (48), 15743–15750.
- (112) Qu, Y.; Chen, B.; Li, Z.; Duan, X.; Wang, L.; Lin, Y.; Yuan, T.; Zhou, F.; Hu, Y.; Yang, Z. Thermal emitting strategy to synthesize atomically dispersed Pt metal sites from bulk Pt metal. *J. Am. Chem. Soc.* **2019**, *141* (11), 4505–4509.
- (113) Qu, Y.; Li, Z.; Chen, W.; Lin, Y.; Yuan, T.; Yang, Z.; Zhao, C.; Wang, J.; Zhao, C.; Wang, X. Direct transformation of bulk copper into copper single sites via emitting and trapping of atoms. *Nat. Catal.* **2018**, *1* (10), 781–786.
- (114) Wei, S.; Li, A.; Liu, J.-C.; Li, Z.; Chen, W.; Gong, Y.; Zhang, Q.; Cheong, W.-C.; Wang, Y.; Zheng, L. Direct observation of noble metal nanoparticles transforming to thermally stable single atoms. *Nat. Nanotechnol.* **2018**, *13* (9), 856–861.
- (115) Wang, S.; Yan, N. X-ray Absorption Spectroscopy: An Indispensable Tool to Study Single-Atom Catalysts. *Synchro. Rad. News* **2020**, 33 (5), 18–26.
- (116) Pan, Y.; Lin, R.; Chen, Y.; Liu, S.; Zhu, W.; Cao, X.; Chen, W.; Wu, K.; Cheong, W.-C.; Wang, Y. Design of single-atom $Co-N_5$ catalytic site: a robust electrocatalyst for CO_2 reduction with nearly 100% CO selectivity and remarkable stability. *J. Am. Chem. Soc.* **2018**, 140 (12), 4218–4221.
- (117) Teo, B. K. EXAFS: basic principles and data analysis; Springer Science & Business Media, 2012; Vol. 9.
- (118) Zhou, Y.; Yang, W.; Utetiwabo, W.; Lian, Y.-m.; Yin, X.; Zhou, L.; Yu, P.; Chen, R.; Sun, S. Revealing of active sites and catalytic mechanism in N-coordinated Fe, Ni dual-doped carbon with superior acidic oxygen reduction than single-atom catalyst. *J. Phys. Chem. Lett.* **2020**, *11* (4), 1404–1410.
- (119) Feiters, M. C.; Meyer-Klaucke, W. X-ray absorption and emission spectroscopy in biology. *Practical Approaches to Biological Inorganic Chemistry*; Elsevier, 2020; pp 229–273.

- (120) Li, X.; Yang, X.; Zhang, J.; Huang, Y.; Liu, B. In situ/operando techniques for characterization of single-atom catalysts. *ACS Catal.* **2019**, 9 (3), 2521–2531.
- (121) DeRita, L.; Dai, S.; Lopez-Zepeda, K.; Pham, N.; Graham, G. W.; Pan, X.; Christopher, P. Catalyst architecture for stable single atom dispersion enables site-specific spectroscopic and reactivity measurements of CO adsorbed to Pt atoms, oxidized Pt clusters, and metallic Pt clusters on TiO₂. *J. Am. Chem. Soc.* **2017**, *139* (40), 14150–14165.
- (122) Boccuzzi, F.; Chiorino, A.; Manzoli, M. FTIR study of the electronic effects of CO adsorbed on gold nanoparticles supported on titania. *Surf. Sci.* **2000**, *454*, 942–946.
- (123) Cortés-Arriagada, D.; Villegas-Escobar, N.; Ortega, D. E. Fedoped graphene nanosheet as an adsorption platform of harmful gas molecules (CO, CO₂, SO₂ and H₂S), and the co-adsorption in O₂ environments. *Appl. Surf. Sci.* **2018**, 427, 227–236.
- (124) Ma, J.; Li, L.; Ren, J.; Li, R. CO adsorption on activated carbon-supported Cu-based adsorbent prepared by a facile route. *Sep. Purif. Technol.* **2010**, 76 (1), 89–93.
- (125) Beniya, A.; Higashi, S. Towards dense single-atom catalysts for future automotive applications. *Nat. Catal.* **2019**, 2 (7), 590–602.
- (126) Boucher, M. B.; Zugic, B.; Cladaras, G.; Kammert, J.; Marcinkowski, M. D.; Lawton, T. J.; Sykes, E. C. H.; Flytzani-Stephanopoulos, M. Single atom alloy surface analogs in $Pd_{0.18}Cu_{15}$ nanoparticles for selective hydrogenation reactions. *Phys. Chem. Chem. Phys.* **2013**, *15* (29), 12187–12196.
- (127) Liu, Q.; Zhang, Z. Platinum single-atom catalysts: a comparative review towards effective characterization. *Catal. Sci. Technol.* **2019**, 9 (18), 4821–4834.
- (128) Muller, D. A. Structure and bonding at the atomic scale by scanning transmission electron microscopy. *Nat. Mater.* **2009**, 8 (4), 263–270.
- (129) Pan, Y.; Chen, Y.; Wu, K.; Chen, Z.; Liu, S.; Cao, X.; Cheong, W.-C.; Meng, T.; Luo, J.; Zheng, L. Regulating the coordination structure of single-atom Fe-N_xC_y catalytic sites for benzene oxidation. *Nat. Commun.* **2019**, *10*, 4290.
- (130) Chen, Y.; Huang, Z.; Ma, Z.; Chen, J.; Tang, X. Fabrication, characterization, and stability of supported single-atom catalysts. *Catal. Sci. Technol.* **2017**, 7 (19), 4250–4258.
- (131) VahidMohammadi, A.; Rosen, J.; Gogotsi, Y. The world of two-dimensional carbides and nitrides (MXenes). *Science* **2021**, 372 (6547), eabf1581.
- (132) Ghim, D.; Chou, P.-I.; Chae, S. H.; Jun, Y.-S. Effects of MoS_2 Layer Thickness on Its Photochemically Driven Oxidative Dissolution. *Environ. Sci. Technol.* **2021**, *55* (20), 13759–13769.
- (133) Ding, M.; Chen, S.; Liu, X. Q.; Sun, L. B.; Lu, J.; Jiang, H. L. Metal—organic framework-templated catalyst: synergy in multiple sites for catalytic CO_2 fixation. *ChemSusChem* **2017**, *10* (9), 1898–1903.
- (134) Côté, A. P.; Benin, A. I.; Ockwig, N. W.; O'Keeffe, M.; Matzger, A. J.; Yaghi, O. M. Porous, crystalline, covalent organic frameworks. *Science* **2005**, 310 (5751), 1166–1170.
- (135) Chen, Y.; Ji, S.; Wang, Y.; Dong, J.; Chen, W.; Li, Z.; Shen, R.; Zheng, L.; Zhuang, Z.; Wang, D. Isolated single iron atoms anchored on N-doped porous carbon as an efficient electrocatalyst for the oxygen reduction reaction. *Angew. Chem.* **2017**, *129* (24), 7041–7045.
- (136) Hu, J.; Li, Y.; Zou, Y.; Lin, L.; Li, B.; Li, X.-y. Transition metal single-atom embedded on N-doped carbon as a catalyst for peroxymonosulfate activation: A DFT study. *Chemical Engineering Journal* **2022**, 437, 135428.
- (137) Evans, D. F.; Upton, M. W. Studies on singlet oxygen in aqueous solution. Part 3. The decomposition of peroxy-acids. *J. Chem. Soc., Dalton Trans.* 1985, No. 6, 1151–1153.
- (138) Flanagan, J.; Griffith, W. P.; Skapski, A. C. The active principle of Caro's acid, HSO₅⁻: X-ray crystal structure of KHSO₅· H₂O. *J. Chem. Soc. Chem. Comm.* **1984**, No. 23, 1574–1575.
- (139) Chen, Z.; Li, X.; Zhang, S.; Jin, J.; Song, X.; Wang, X.; Tratnyek, P. G. Overlooked role of peroxides as free radical precursors in advanced oxidation processes. *Environ. Sci. Technol.* **2019**, *53* (4), 2054–2062.

- (140) Kolthoff, I.; Miller, I. The chemistry of persulfate. I. The kinetics and mechanism of the decomposition of the persulfate ion in aqueous medium1. *J. Am. Chem. Soc.* **1951**, *73* (7), 3055–3059.
- (141) Yang, S.; Wang, P.; Yang, X.; Shan, L.; Zhang, W.; Shao, X.; Niu, R. Degradation efficiencies of azo dye Acid Orange 7 by the interaction of heat, UV and anions with common oxidants: persulfate, peroxymonosulfate and hydrogen peroxide. *J. Hazard. Mater.* **2010**, 179 (1–3), 552–558.
- (142) Benson, S. W. Thermochemistry and kinetics of sulfur-containing molecules and radicals. *Chem. Rev.* **1978**, 78 (1), 23–35.
- (143) Duan, X.; Sun, H.; Ao, Z.; Zhou, L.; Wang, G.; Wang, S. Unveiling the active sites of graphene-catalyzed peroxymonosulfate activation. *Carbon* **2016**, *107*, 371–378.
- (144) Duan, X.; Sun, H.; Wang, S. Metal-free carbocatalysis in advanced oxidation reactions. *Acc. Chem. Res.* **2018**, *51* (3), *678*–687. (145) Gao, Y.; Chen, Z.; Zhu, Y.; Li, T.; Hu, C. New insights into the generation of singlet oxygen in the metal-free peroxymonosulfate
- generation of singlet oxygen in the metal-free peroxymonosulfate activation process: Important role of electron-deficient carbon atoms. *Environ. Sci. Technol.* **2020**, 54 (2), 1232–1241.
- (146) Wang, Y.; Ao, Z.; Sun, H.; Duan, X.; Wang, S. Activation of peroxymonosulfate by carbonaceous oxygen groups: experimental and density functional theory calculations. *Appl. Catal. B Environ.* **2016**, 198, 295–302.
- (147) Zhang, P.; Yang, Y.; Duan, X.; Liu, Y.; Wang, S. Density functional theory calculations for insight into the heterocatalyst reactivity and mechanism in persulfate-based advanced oxidation reactions. ACS Catal. 2021, 11 (17), 11129–11159.
- (148) Rodriguez-Reinoso, F. The role of carbon materials in heterogeneous catalysis. *Carbon* **1998**, *36* (3), 159–175.
- (149) Jiang, D.-e.; Sumpter, B. G.; Dai, S. Unique chemical reactivity of a graphene nanoribbon's zigzag edge. *J. Chem. Phys.* **2007**, *126* (13), 134701
- (150) Lee, G.; Cho, K. Electronic structures of zigzag graphene nanoribbons with edge hydrogenation and oxidation. *Phys. Rev. B* **2009**, 79 (16), 165440.
- (151) Su, C.; Acik, M.; Takai, K.; Lu, J.; Hao, S.-j.; Zheng, Y.; Wu, P.; Bao, Q.; Enoki, T.; Chabal, Y. J. Probing the catalytic activity of porous graphene oxide and the origin of this behaviour. *Nat. Commun.* **2012**, *3*, 1298.
- (152) Deng, D.; Yu, L.; Pan, X.; Wang, S.; Chen, X.; Hu, P.; Sun, L.; Bao, X. Size effect of graphene on electrocatalytic activation of oxygen. *Chem. Commun.* **2011**, 47 (36), 10016–10018.
- (153) Zhang, H.; Lv, K.; Fang, B.; Forster, M. C.; Dervişoğlu, R.; Andreas, L. B.; Zhang, K.; Chen, S. Crucial role for oxygen functional groups in the oxygen reduction reaction electrocatalytic activity of nitrogen-doped carbons. *Electrochim. Acta* **2018**, *292*, 942–950.
- (154) Edwards, J. O.; Pater, R. H.; Curclf, R.; Furia, F. D. On the formation and reactivity of dioxirane intermediates in the reaction of peroxoanions with organic substrates. *Photochem. Photobiol.* **1979**, 30 (1), 63–70.
- (155) Han, C.; Duan, X.; Zhang, M.; Fu, W.; Duan, X.; Ma, W.; Liu, S.; Wang, S.; Zhou, X. Role of electronic properties in partition of radical and nonradical processes of carbocatalysis toward peroxymonosulfate activation. *Carbon* **2019**, *153*, 73–80.
- (156) Morimoto, N.; Kubo, T.; Nishina, Y. Tailoring the oxygen content of graphite and reduced graphene oxide for specific applications. *Sci. Reports* **2016**, *6*, 21715.
- (157) Chen, H.; Sun, F.; Wang, J.; Li, W.; Qiao, W.; Ling, L.; Long, D. Nitrogen doping effects on the physical and chemical properties of mesoporous carbons. *J. Phys. Chem. C* **2013**, *117* (16), 8318–8328.
- (158) Hu, Y.; Liu, H.; Ke, Q.; Wang, J. Effects of nitrogen doping on supercapacitor performance of a mesoporous carbon electrode produced by a hydrothermal soft-templating process. *J. Mater. Chem. A* **2014**, 2 (30), 11753–11758.
- (159) Ismagilov, Z. R.; Shalagina, A. E.; Podyacheva, O. Y.; Ischenko, A. V.; Kibis, L. S.; Boronin, A. I.; Chesalov, Y. A.; Kochubey, D. I.; Romanenko, A. I.; Anikeeva, O. B. Structure and electrical conductivity of nitrogen-doped carbon nanofibers. *Carbon* **2009**, *47* (8), 1922–1929.

- (160) Lim, D.-H.; Wilcox, J. DFT-based study on oxygen adsorption on defective graphene-supported Pt nanoparticles. *J. Phys. Chem. C* **2011**, *115* (46), 22742–22747.
- (161) Roche, I.; Chaînet, E.; Chatenet, M.; Vondrák, J. Carbon-supported manganese oxide nanoparticles as electrocatalysts for the oxygen reduction reaction (ORR) in alkaline medium: physical characterizations and ORR mechanism. *J. Phys. Chem. C* **2007**, *111* (3), 1434–1443.
- (162) Shin, K.; Kim, D. H.; Yeo, S. C.; Lee, H. M. Structural stability of AgCu bimetallic nanoparticles and their application as a catalyst: A DFT study. *Catal. Today* **2012**, *185* (1), 94–98.
- (163) Staykov, A.; Nishimi, T.; Yoshizawa, K.; Ishihara, T. Oxygen activation on nanometer-size gold nanoparticles. *J. Phys. Chem. C* **2012**, *116* (30), 15992–16000.
- (164) Wang, L.; Roudgar, A.; Eikerling, M. Ab initio study of stability and site-specific oxygen adsorption energies of Pt nanoparticles. *J. Phys. Chem. C* **2009**, *113* (42), 17989–17996.
- (165) Gao, J.; Liu, B. Progress of electrochemical hydrogen peroxide synthesis over single atom catalysts. *ACS Mater. Lett.* **2020**, 2 (8), 1008–1024.
- (166) Wang, C.; Jia, S.; Zhang, Y.; Nian, Y.; Wang, Y.; Han, Y.; Liu, Y.; Ren, H.; Wu, S.; Yao, K. Catalytic reactivity of Co_3O_4 with different facets in the hydrogen abstraction of phenol by persulfate. *Appl. Catal. B Environ.* **2020**, 270, 118819.
- (167) Li, S.; Hou, Y.; Chen, Q.; Zhang, X.; Cao, H.; Huang, Y. Promoting active sites in MOF-derived homobimetallic hollow nanocages as a high-performance multifunctional nanozyme catalyst for biosensing and organic pollutant degradation. *ACS Appl. Mater. Interfaces* **2020**, *12* (2), 2581–2590.
- (168) Li, H.; Zhang, P.; Guo, Y.; Jia, J.; Wang, S.; Duan, X.; Cui, F.; Gao, S.; Tian, J. Iron-doped cuprous oxides toward accelerated nonradical oxidation: Doping induced controlled facet transformation and optimized electronic structure. *Chem. Eng. J.* **2021**, 407, 127172.
- (169) He, J.; Wan, Y.; Zhou, W. ZIF-8 derived Fe—N coordination moieties anchored carbon nanocubes for efficient peroxymonosulfate activation via non-radical pathways: Role of FeNx sites. *J. Hazard. Mater.* **2021**, 405, 124199.
- (170) Yu, J.; Zeng, T.; Wang, H.; Zhang, H.; Sun, Y.; Chen, L.; Song, S.; Li, L.; Shi, H. J. C. E. J. Oxygen-defective MnO₂–x rattle-type microspheres mediated singlet oxygen oxidation of organics by peroxymonosulfate activation. *Chem. Eng. J.* **2020**, 394, 124458.
- (171) Liu, L.; Liu, Q.; Wang, Y.; Huang, J.; Wang, W.; Duan, L.; Yang, X.; Yu, X.; Han, X.; Liu, N. Nonradical activation of peroxydisulfate promoted by oxygen vacancy-laden NiO for catalytic phenol oxidative polymerization. *Appl. Catal. B Environ.* **2019**, 254, 166–173.
- (172) Yang, J.; Zeng, D.; Li, J.; Dong, L.; Ong, W.-J.; He, Y. A highly efficient Fenton-like catalyst based on isolated diatomic Fe-Co anchored on N-doped porous carbon. *Chem. Eng. J.* **2021**, *404*, 126376.
- (173) Yang, L.; Yang, H.; Yin, S.; Wang, X.; Xu, M.; Lu, G.; Liu, Z.; Sun, H. Fe Single-Atom Catalyst for Efficient and Rapid Fenton-Like Degradation of Organics and Disinfection against Bacteria. *Small* **2022**, *18*, 2104941.
- (174) Zhang, L. S.; Jiang, X. H.; Zhong, Z. A.; Tian, L.; Sun, Q.; Cui, Y. T.; Lu, X.; Zou, J. P.; Luo, S. L. Carbon Nitride Supported High-Loading Fe Single-Atom Catalyst for Activation of Peroxymonosulfate to Generate $^{1}\mathrm{O}_{2}$ with 100% Selectivity. *Angew. Chem.* **2021**, *60* (40), 21751–21755.
- (175) Liu, J.; He, H.; Shen, Z.; Wang, H. H.; Li, W. Photoassisted highly efficient activation of persulfate over a single-atom Cu catalyst for tetracycline degradation: process and mechanism. *J. Hazard. Mater.* **2022**, *429*, 128398.
- (176) Wu, H.; Yan, J.; Xu, X.; Yuan, Q.; Wang, J.; Cui, J.; Lin, A. Synergistic effects for boosted persulfate activation in a designed Fe—Cu dual-atom site catalyst. *Chem. Eng. J.* **2022**, 428, 132611.
- (177) Teng, Z.; Cai, W.; Sim, W.; Zhang, Q.; Wang, C.; Su, C.; Ohno, T. Photoexcited single metal atom catalysts for heterogeneous photocatalytic H₂O₂ production: pragmatic guidelines for predicting charge separation. *Appl. Catal. B Environ.* **2021**, 282, 119589.

- (178) Cao, H.; Xia, G.-J.; Chen, J.-W.; Yan, H.-M.; Huang, Z.; Wang, Y.-G. Mechanistic insight into the oxygen reduction reaction on the $Mn-N_4/C$ single-atom catalyst: the role of the solvent environment. *J. Phys. Chem. C* **2020**, 124 (13), 7287–7294.
- (179) Huang, L.-Z.; Zhou, C.; Shen, M.; Gao, E.; Zhang, C.; Hu, X.-M.; Chen, Y.; Xue, Y.; Liu, Z. Persulfate activation by two-dimensional MoS₂ confining single Fe atoms: Performance, mechanism and DFT calculations. *J. Hazard. Mater.* **2020**, 389, 122137.
- (180) Yang, J.; Zeng, D.; Zhang, Q.; Cui, R.; Hassan, M.; Dong, L.; Li, J.; He, Y. Single Mn atom anchored on N-doped porous carbon as highly efficient Fenton-like catalyst for the degradation of organic contaminants. *Appl. Catal. B Environ.* **2020**, *279*, 119363.
- (181) Chu, C.; Yang, J.; Zhou, X.; Huang, D.; Qi, H.; Weon, S.; Li, J.; Elimelech, M.; Wang, A.; Kim, J.-H. Cobalt Single Atoms on Tetrapyridomacrocyclic Support for Efficient Peroxymonosulfate Activation. *Environ. Sci. Technol.* **2021**, *55* (2), 1242–1250.
- (182) Liang, C.; Su, H.-W. Identification of sulfate and hydroxyl radicals in thermally activated persulfate. *Ind. Eng. Chem. Res.* **2009**, 48 (11), 5558–5562.
- (183) Wei, Z.; Villamena, F. A.; Weavers, L. K. Kinetics and mechanism of ultrasonic activation of persulfate: an in situ EPR spin trapping study. *Environ. Sci. Technol.* **2017**, *51* (6), 3410–3417.
- (184) Chen, X.; Oh, W.-D.; Hu, Z.-T.; Sun, Y.-M.; Webster, R. D.; Li, S.-Z.; Lim, T.-T. Enhancing sulfacetamide degradation by peroxymonosulfate activation with N-doped graphene produced through delicately-controlled nitrogen functionalization via tweaking thermal annealing processes. *Appl. Catal. B Environ.* **2018**, 225, 243–257.
- (185) Huang, Z.; Bao, H.; Yao, Y.; Lu, W.; Chen, W. Novel green activation processes and mechanism of peroxymonosulfate based on supported cobalt phthalocyanine catalyst. *Appl. Catal. B Environ.* **2014**, 154, 36–43.
- (186) Das, T. N.; Huie, R. E.; Neta, P. Reduction potentials of $SO_3^{\bullet-}$, $SO_5^{\bullet-}$, and $S_4O_6^{\bullet-3}$ -radicals in aqueous solution. *J. Phys. Chem. A* **1999**, 103 (18), 3581–3588.
- (187) Liu, H.; Bruton, T. A.; Doyle, F. M.; Sedlak, D. L. In situ chemical oxidation of contaminated groundwater by persulfate: decomposition by Fe (III)-and Mn (IV)-containing oxides and aquifer materials. *Environ. Sci. Technol.* **2014**, *48* (17), 10330–10336.
- (188) Liu, H.; Bruton, T. A.; Li, W.; Buren, J. V.; Prasse, C.; Doyle, F. M.; Sedlak, D. L. Oxidation of benzene by persulfate in the presence of Fe (III)-and Mn (IV)-containing oxides: stoichiometric efficiency and transformation products. *Environ. Sci. Technol.* **2016**, *50* (2), 890–898.
- (189) Oh, W.-D.; Lim, T.-T. Design and application of heterogeneous catalysts as peroxydisulfate activator for organics removal: an overview. *Chem. Eng. J.* **2019**, 358, 110–133.
- (190) Clarke, K.; Edge, R.; Land, E.; Navaratnam, S.; Truscott, T. The sulphate radical is not involved in aqueous radiation oxidation processes. *Radiat. Phys. Chem.* **2008**, *77* (1), 49–52.
- (191) Zhu, C.; Zhu, F.; Liu, C.; Chen, N.; Zhou, D.; Fang, G.; Gao, J. J. E. s. technology, Reductive hexachloroethane degradation by $S_2O_8^{\bullet-}$ with thermal activation of persulfate under anaerobic conditions. *Environ. Sci. Technol.* **2018**, 52 (15), 8548–8557.
- (192) Chen, R.; Pignatello, J. J. Role of quinone intermediates as electron shuttles in Fenton and photoassisted Fenton oxidations of aromatic compounds. *Environ. Sci. Technol.* 1997, 31 (8), 2399–2406.
- (193) Rodriguez, S.; Santos, A.; Romero, A. Oxidation of priority and emerging pollutants with persulfate activated by iron: effect of iron valence and particle size. *Chem. Eng. J.* **2017**, *318*, 197–205.
- (194) Rodriguez, S.; Vasquez, L.; Costa, D.; Romero, A.; Santos, A. Oxidation of Orange G by persulfate activated by Fe (II), Fe (III) and zero valent iron (ZVI). *Chemosphere* **2014**, *101*, 86–92.
- (195) Sun, Z.; Li, S.; Ding, H.; Zhu, Y.; Wang, X.; Liu, H.; Zhang, Q.; Zhao, C. Electrochemical/Fe³⁺/peroxymonosulfate system for the degradation of Acid Orange 7 adsorbed on activated carbon fiber cathode. *Chemosphere* **2020**, *241*, 125125.
- (196) Chen, L.; Ma, J.; Li, X.; Zhang, J.; Fang, J.; Guan, Y.; Xie, P. Strong enhancement on Fenton oxidation by addition of hydroxylamine to accelerate the ferric and ferrous iron cycles. *Environ. Sci. Technol.* **2011**, 45 (9), 3925–3930.

- (197) Zou, J.; Ma, J.; Chen, L.; Li, X.; Guan, Y.; Xie, P.; Pan, C. Rapid acceleration of ferrous iron/peroxymonosulfate oxidation of organic pollutants by promoting Fe (III)/Fe (II) cycle with hydroxylamine. *Environ. Sci. Technol.* **2013**, 47 (20), 11685–11691.
- (198) Armstrong, D. A.; Huie, R. E.; Koppenol, W. H.; Lymar, S. V.; Merényi, G.; Neta, P.; Ruscic, B.; Stanbury, D. M.; Steenken, S.; Wardman, P. Standard electrode potentials involving radicals in aqueous solution: inorganic radicals (IUPAC Technical Report). *Pure Appl. Chem.* **2015**, 87 (11–12), 1139–1150.
- (199) Chen, M.; Wang, N.; Zhu, L. Single-atom dispersed Co-NC: a novel adsorption-catalysis bifunctional material for rapid removing bisphenol A. *Catal. Today* **2020**, *348*, 187–193.
- (200) Du, N.; Liu, Y.; Li, Q.; Miao, W.; Wang, D.; Mao, S. Peroxydisulfate activation by atomically-dispersed Fe-Nx on N-doped carbon: Mechanism of singlet oxygen evolution for nonradical degradation of aqueous contaminants. *Chem. Eng. J.* **2021**, *413*, 127545.
- (201) Zhao, X.; Li, X.; Zhu, Z.; Hu, W.; Zhang, H.; Xu, J.; Hu, X.; Zhou, Y.; Xu, M.; Zhang, H. Single-atom Co embedded in BCN matrix to achieve 100% conversion of peroxymonosulfate into singlet oxygen. *Appl. Catal. B Environ.* **2022**, 300, 120759.
- (202) Lyu, Z.; Xu, M.; Wang, J.; Li, A.; Corvini, P. F.-X. Hierarchical nano-vesicles with bimetal-encapsulated for peroxymonosulfate activation: Singlet oxygen-dominated oxidation process. *Chem. Eng. J.* **2022**, 433 (2), 133581.
- (203) Yang, Y.; Banerjee, G.; Brudvig, G. W.; Kim, J.-H.; Pignatello, J. J. Oxidation of organic compounds in water by unactivated peroxymonosulfate. *Environ. Sci. Technol.* **2018**, *52* (10), 5911–5919.
- (204) Buxton, G. V.; Greenstock, C. L.; Helman, W. P.; Ross, A. B. Critical review of rate constants for reactions of hydrated electrons, hydrogen atoms and hydroxyl radicals $(\cdot OH/\cdot O^-)$ in aqueous solution. *J. Phys. Chem. Ref. Data* **1988**, *17* (2), 513–886.
- (205) Wilkinson, F.; Helman, W. P.; Ross, A. B. Rate constants for the decay and reactions of the lowest electronically excited singlet state of molecular oxygen in solution. An expanded and revised compilation. *J. Phys. Chem. Ref. Data* **1995**, 24 (2), 663–677.
- (206) Miyamoto, S.; Martinez, G. R.; Medeiros, M. H.; Di Mascio, P. Singlet molecular oxygen generated from lipid hydroperoxides by the Russell mechanism: studies using ¹⁸O-labeled linoleic acid hydroperoxide and monomol light emission measurements. *J. Am. Chem. Soc.* **2003**, *125* (20), *6172–6179*.
- (207) Zhou, Y.; Jiang, J.; Gao, Y.; Ma, J.; Pang, S.-Y.; Li, J.; Lu, X.-T.; Yuan, L.-P. Activation of peroxymonosulfate by benzoquinone: a novel nonradical oxidation process. *Environ. Sci. Technol.* **2015**, 49 (21), 12941–12950.
- (208) Khan, A. U.; Kovacic, D.; Kolbanovskiy, A.; Desai, M.; Frenkel, K.; Geacintov, N. E. The decomposition of peroxynitrite to nitroxyl anion (NO⁻) and singlet oxygen in aqueous solution. *Proc. Nat. Acad. Sci.* **2000**, *97* (7), 2984–2989.
- (209) You, Y. Chemical tools for the generation and detection of singlet oxygen. Org. Biomolecul. Chem. 2018, 16 (22), 4044–4060.
- (210) Lindig, B. A.; Rodgers, M. A.; Schaap, A. P. Determination of the lifetime of singlet oxygen in water-d2 using 9, 10-anthracenedipropionic acid, a water-soluble probe. *J. Am. Chem. Soc.* **1980**, *102* (17), 5590–5593.
- (211) Shellum, C. L.; Birks, J. W. Photochemical amplifier for liquid chromatography based on singlet oxygen sensitization. *Anal. Chem.* **1987**, 59 (14), 1834–1841.
- (212) Young, R. H.; Wehrly, K.; Martin, R. L. Solvent effects in dyesensitized photooxidation reactions. *J. Am. Chem. Soc.* **1971**, 93 (22), 5774–5779.
- (213) Umezawa, N.; Tanaka, K.; Urano, Y.; Kikuchi, K.; Higuchi, T.; Nagano, T. Novel fluorescent probes for singlet oxygen. *Angew. Chem.* **1999**, 38 (19), 2899–2901.
- (214) Flors, C.; Fryer, M. J.; Waring, J.; Reeder, B.; Bechtold, U.; Mullineaux, P. M.; Nonell, S.; Wilson, M. T.; Baker, N. R. Imaging the production of singlet oxygen in vivo using a new fluorescent sensor, Singlet Oxygen Sensor Green®. *J. Exp. Botany* **2006**, *57* (8), 1725–1734.

- (215) Eglen, R. M.; Reisine, T.; Roby, P.; Rouleau, N.; Illy, C.; Bossé, R.; Bielefeld, M. The use of AlphaScreen technology in HTS: current status. *Current Chem. Genom.* **2008**, *1*, 2.
- (216) Bielefeld-Sevigny, M. AlphaLISA immunoassay platform—the "no-wash" high-throughput alternative to ELISA. *Assay Drug Develop. Technol.* **2009**, *7* (1), 90–92.
- (217) Matsumoto, M.; Watanabe, N.; Shiono, T.; Suganuma, H.; Matsubara, J. Chemiluminescence of spiro [1, 2-dioxetane-3, 1'-dihydroisobenzofuran] s, spiro [1, 2-dioxetane-3, 1'-isochroman] s and a spiro [1, 2-dioxetane-3, 1'-(2-benzoxepane)]. *Tetra. Lett.* **1997**, 38 (33), 5825–5828.
- (218) Kazakov, D. V.; Safarov, F. E. A novel chemiluminescence from the reaction of singlet oxygen with β -diketonates of europium (III), neodymium (III) and ytterbium (III). *Photochem. Photobiol. Sci.* **2014**, 13 (12), 1646–1649.
- (219) Liu, S.; Zhang, Z.; Huang, F.; Liu, Y.; Feng, L.; Jiang, J.; Zhang, L.; Qi, F.; Liu, C. Carbonized polyaniline activated peroxymonosulfate (PMS) for phenol degradation: Role of PMS adsorption and singlet oxygen generation. *Appl. Catal. B Environ.* **2021**, 286, 119921.
- (220) Yun, E.-T.; Lee, J. H.; Kim, J.; Park, H.-D.; Lee, J. Identifying the nonradical mechanism in the peroxymonosulfate activation process: singlet oxygenation versus mediated electron transfer. *Environ. Sci. Technol.* **2018**, 52 (12), 7032–7042.
- (221) Lange, A.; Brauer, H.-D. On the formation of dioxiranes and of singlet oxygen by the ketone-catalysed decomposition of Caro's acid. *J. Chem. Soc., Perkin Trans.* **1996**, No. 5, 805–811.
- (222) Montgomery, R. E. Catalysis of peroxymonosulfate reactions by ketones. J. Am. Chem. Soc. 1974, 96 (25), 7820–7821.
- (223) Chen, C.; Ma, T.; Shang, Y.; Gao, B.; Jin, B.; Dan, H.; Li, Q.; Yue, Q.; Li, Y.; Wang, Y. In-situ pyrolysis of Enteromorpha as carbocatalyst for catalytic removal of organic contaminants: Considering the intrinsic N/Fe in Enteromorpha and non-radical reaction. *Appl. Catal. B Environ.* **2019**, *250*, 382–395.
- (224) Liu, Y.; Guo, H.; Zhang, Y.; Tang, W.; Cheng, X.; Li, W. Heterogeneous activation of peroxymonosulfate by sillenite Bi₂₅FeO₄₀: singlet oxygen generation and degradation for aquatic levofloxacin. *Chem. Eng. J.* **2018**, 343, 128–137.
- (225) Furman, O. S.; Teel, A. L.; Watts, R. J. Mechanism of base activation of persulfate. *Environ. Sci. Technol.* **2010**, 44 (16), 6423–6428.
- (226) Sawyer, D. T.; Valentine, J. S. How super is superoxide? *Acc. Chem. Res.* **1981**, *14* (12), 393–400.
- (227) Zhu, S.; Li, X.; Kang, J.; Duan, X.; Wang, S. Persulfate activation on crystallographic manganese oxides: mechanism of singlet oxygen evolution for nonradical selective degradation of aqueous contaminants. *Environ. Sci. Technol.* **2019**, *53* (1), 307–315.
- (228) Gao, Y.; Wu, T.; Yang, C.; Ma, C.; Zhao, Z.; Wu, Z.; Cao, S.; Geng, W.; Wang, Y.; Yao, Y. Activity Trends and Mechanisms in Peroxymonosulfate-Assisted Catalytic Production of Singlet Oxygen over Atomic Metal-N-C Catalysts. *Angew. Chem.* **2021**, *60* (41), 22513–22521.
- (229) Wang, M.; Cui, Y.; Cao, H.; Wei, P.; Chen, C.; Li, X.; Xu, J.; Sheng, G. Activating peroxydisulfate with Co₃O₄/NiCo₂O₄ double-shelled nanocages to selectively degrade bisphenol A–A nonradical oxidation process. *Appl. Catal. B Environ.* **2021**, 282, 119585.
- (230) Ren, W.; Xiong, L.; Nie, G.; Zhang, H.; Duan, X.; Wang, S. Insights into the electron-transfer regime of peroxydisulfate activation on carbon nanotubes: The role of oxygen functional groups. *Environ. Sci. Technol.* **2020**, 54 (2), 1267–1275.
- (231) Duan, P.; Pan, J.; Du, W.; Yue, Q.; Gao, B.; Xu, X. Activation of peroxymonosulfate via mediated electron transfer mechanism on single-atom Fe catalyst for effective organic pollutants removal. *Appl. Catal. B Environ.* **2021**, 299, 120714.
- (232) Li, Z.; Li, K.; Ma, S.; Dang, B.; Li, Y.; Fu, H.; Du, J.; Meng, Q. Activation of peroxymonosulfate by iron-biochar composites: Comparison of nanoscale Fe with single-atom Fe. *J. Colloid Interface Sci.* **2021**, 582, 598–609.

- (233) Li, Y.; Kong, T.; Shen, S. Artificial photosynthesis with polymeric carbon nitride: when meeting metal nanoparticles, single atoms, and molecular complexes. *Small* **2019**, *15* (32), 1900772.
- (234) Peng, Y.; Lu, B.; Chen, S. Carbon-supported single atom catalysts for electrochemical energy conversion and storage. *Adv. Mater.* **2018**, *30* (48), 1801995.
- (235) Su, P.; Pei, W.; Wang, X.; Ma, Y.; Jiang, Q.; Liang, J.; Zhou, S.; Zhao, J.; Liu, J.; Lu, G. Q. Exceptional electrochemical HER performance with enhanced electron transfer between Ru nanoparticles and single atoms dispersed on a carbon substrate. *Angew. Chem.* **2021**, 133 (29), 16180–16186.
- (236) Subramanian, V.; Wolf, E. E.; Kamat, P. V. Catalysis with TiO₂/gold nanocomposites. Effect of metal particle size on the Fermi level equilibration. *J. Am. Chem. Soc.* **2004**, *126* (15), 4943–4950.
- (237) Gao, Y.; Zhou, Y.; Pang, S.-Y.; Jiang, J.; Shen, Y.-M.; Song, Y.; Duan, J.-B.; Guo, Q. Enhanced peroxymonosulfate activation via complexed Mn (II): A novel non-radical oxidation mechanism involving manganese intermediates. *Water Res.* **2021**, *193*, 116856.
- (238) Zong, Y.; Zhang, H.; Zhang, X.; Shao, Y.; Zeng, Y.; Ji, W.; Xu, L.; Wu, D. Highly selective oxidation of organic contaminants in the Ru^{III}-activated peroxymonosulfate process: The dominance of Ru^VO species. *Chemosphere* **2021**, 285, 131544.
- (239) Zong, Y.; Guan, X.; Xu, J.; Feng, Y.; Mao, Y.; Xu, L.; Chu, H.; Wu, D. Unraveling the overlooked involvement of high-valent cobalt-oxo species generated from the cobalt (II)-activated peroxymonosulfate process. *Environ. Sci. Technol.* **2020**, *54* (24), 16231–16239.
- (240) Kang, H.; Lee, D.; Lee, K.-M.; Kim, H.-H.; Lee, H.; Kim, M. S.; Lee, C. Nonradical activation of peroxymonosulfate by hematite for oxidation of organic compounds: A novel mechanism involving high-valent iron species. *Chem. Eng. J.* **2021**, 426, 130743.
- (241) Li, H.; Shan, C.; Li, W.; Pan, B. Peroxymonosulfate activation by iron (III)-tetraamidomacrocyclic ligand for degradation of organic pollutants via high-valent iron-oxo complex. *Water Res.* **2018**, *147*, 233–241.
- (242) Wang, Z.; Qiu, W.; Pang, S.; Gao, Y.; Zhou, Y.; Cao, Y.; Jiang, J. Relative contribution of ferryl ion species (Fe (IV)) and sulfate radical formed in nanoscale zero valent iron activated peroxydisulfate and peroxymonosulfate processes. *Water Res.* **2020**, *172*, 115504.
- (243) Li, H.; Shan, C.; Pan, B. Fe (III)-doped g-C₃N₄ mediated peroxymonosulfate activation for selective degradation of phenolic compounds via high-valent iron-oxo species. *Environ. Sci. Technol.* **2018**, 52 (4), 2197–2205.
- (244) Peng, L.; Duan, X.; Shang, Y.; Gao, B.; Xu, X. Engineered carbon supported single iron atom sites and iron clusters from Fe-rich Enteromorpha for Fenton-like reactions via nonradical pathways. *Appl. Catal. B Environ.* **2021**, 287, 119963.
- (245) Peng, X.; Wu, J.; Zhao, Z.; Wang, X.; Dai, H.; Xu, L.; Xu, G.; Jian, Y.; Hu, F. Activation of peroxymonosulfate by single-atom Fe-g- C_3N_4 catalysts for high efficiency degradation of tetracycline via nonradical pathways: Role of high-valent iron-oxo species and Fe-Nx sites. *Chem. Eng. J.* **2022**, *427*, 130803.
- (246) Zhang, B.; Li, X.; Akiyama, K.; Bingham, P. A.; Kubuki, S. Elucidating the Mechanistic Origin of a Spin State-Dependent FeN_x —C Catalyst toward Organic Contaminant Oxidation via Peroxymonosulfate Activation. *Environ. Sci. Technol.* **2022**, *56* (2), 1321–1330.
- (247) Conocchioli, T.; Hamilton, E., Jr; Sutin, N. The formation of iron (IV) in the oxidation of iron (II). *J. Am. Chem. Soc.* **1965**, 87 (4), 926–927.
- (248) Mártire, D. O.; Caregnato, P.; Furlong, J.; Allegretti, P.; Gonzalez, M. C. Kinetic study of the reactions of oxoiron (IV) with aromatic substrates in aqueous solutions. *Inter. J. Chem. Kinet.* **2002**, 34 (8), 488–494.
- (249) Pestovsky, O.; Bakac, A. Reactivity of aqueous Fe (IV) in hydride and hydrogen atom transfer reactions. *J. Am. Chem. Soc.* **2004**, 126 (42), 13757–13764.
- (250) Wang, Z.; Jiang, J.; Pang, S.; Zhou, Y.; Guan, C.; Gao, Y.; Li, J.; Yang, Y.; Qiu, W.; Jiang, C. Is sulfate radical really generated from peroxydisulfate activated by iron (II) for environmental decontamination? *Environ. Sci. Technol.* **2018**, 52 (19), 11276–11284.

- (251) Li, H.; Shan, C.; Pan, B. Development of Fe-doped g- $C_3N_4/$ graphite mediated peroxymonosulfate activation for degradation of aromatic pollutants via nonradical pathway. *Sci. Total. Environ.* **2019**, 675, 62–72.
- (252) Wang, Z.; Wang, W.; Wang, J.; Yuan, Y.; Wu, Q.; Hu, H. High-Valent Iron-Oxo Species Mediated Cyclic Oxidation through Single-Atom Fe-N6 Sites with High Peroxymonosulfate Utilization Rate. *Appl. Catal. B Environ.* **2022**, 305, 121049.
- (253) Zong, Y.; Shao, Y.; Zeng, Y.; Shao, B.; Xu, L.; Zhao, Z.; Liu, W.; Wu, D. Enhanced Oxidation of Organic Contaminants by Iron (II)-Activated Periodate: The Significance of High-Valent Iron—Oxo Species. *Environ. Sci. Technol.* **2021**, *55* (11), 7634—7642.
- (254) Novak, P.; Kolar, M.; Machala, L.; Siskova, K. M.; Karlicky, F.; Petr, M.; Zboril, R. Transformations of ferrates (iv, v, vi) in liquids: Mössbauer spectroscopy of frozen solutions. *Phys. Chem. Chem. Phys.* **2018**, 20 (48), 30247–30256.
- (255) Wang, Z.; Qiu, W.; Pang, S.-y.; Zhou, Y.; Gao, Y.; Guan, C.; Jiang, J. Further understanding the involvement of Fe (IV) in peroxydisulfate and peroxymonosulfate activation by Fe (II) for oxidative water treatment. *Chem. Eng. J.* **2019**, *371*, 842–847.
- (256) Liu, B.; Guo, W.; Wang, H.; Zheng, S.; Si, Q.; Zhao, Q.; Luo, H.; Ren, N. Peroxymonosulfate activation by cobalt (II) for degradation of organic contaminants via high-valent cobalt-oxo and radical species. *J. Hazard. Mater.* **2021**, *416*, 125679.
- (257) Šišková, K. M.; Jančula, D.; Drahoš, B.; Machala, L.; Babica, P.; Alonso, P. G.; Trávníček, Z.; Tuček, J.; Maršálek, B.; Sharma, V. K. High-valent iron (Fe VI, Fe V, and Fe IV) species in water: Characterization and oxidative transformation of estrogenic hormones. *Phys. Chem. Chem. Phys.* **2016**, *18* (28), 18802–18810.
- (258) Vallejos, S.; Muñoz, A.; Ibeas, S.; Serna, F.; García, F. C.; García, J. M. Solid sensory polymer substrates for the quantification of iron in blood, wine and water by a scalable RGB technique. *J. Mater. Chem. A* **2013**, *1* (48), 15435–15441.
- (259) Liu, X.; Yu, H.; Ji, J.; Chen, Z.; Ran, M.; Zhang, J.; Xing, M. Graphene Oxide-Supported Three-Dimensional Cobalt—Nickel Bimetallic Sponge-Mediated Peroxymonosulfate Activation for Phenol Degradation. ACS EST Engg. 2021, 1 (12), 1705–1714.
- (260) Tian, H.; Wang, Z.; Zhu, T.; Yang, C.; Shi, Y.; Sun, Y. Degradation Prediction and Products of Polycyclic Aromatic Hydrocarbons in Soils by Highly Active Bimetals/AC-Activated Persulfate. ACS EST Engg. 2021, 1 (8), 1183–1192.
- (261) Tan, C.; Gao, N.; Fu, D.; Deng, J.; Deng, L. Efficient degradation of paracetamol with nanoscaled magnetic CoFe₂O₄ and MnFe₂O₄ as a heterogeneous catalyst of peroxymonosulfate. *Sep. Purif. Technol.* **2017**, *175*, 47–57.
- (262) Xu, Y.; Ai, J.; Zhang, H. The mechanism of degradation of bisphenol A using the magnetically separable CuFe₂O₄/peroxymonosulfate heterogeneous oxidation process. *J. Hazard. Mater.* **2016**, 309, 87–96.
- (263) Chen, L.; Zuo, X.; Zhou, L.; Huang, Y.; Yang, S.; Cai, T.; Ding, D. Efficient heterogeneous activation of peroxymonosulfate by facilely prepared Co/Fe bimetallic oxides: kinetics and mechanism. *Chem. Eng. J.* **2018**, *345*, 364–374.
- (264) Ding, Y.; Pan, C.; Peng, X.; Mao, Q.; Xiao, Y.; Fu, L.; Huang, J. Deep mineralization of bisphenol A by catalytic peroxymonosulfate activation with nano CuO/Fe₃O₄ with strong Cu-Fe interaction. *Chem. Eng. J.* **2020**, 384, 123378.
- (265) Huang, G.-X.; Wang, C.-Y.; Yang, C.-W.; Guo, P.-C.; Yu, H.-Q. Degradation of bisphenol A by peroxymonosulfate catalytically activated with $\mathrm{Mn_{1.\,8}Fe_{1.\,2}O_4}$ nanospheres: synergism between Mn and Fe. *Environ. Sci. Technol.* **2017**, *51* (21), 12611–12618.
- (266) Li, M.-H.; Lin, K.-Y. A.; Yang, M.-T.; Thanh, B. X.; Tsang, D. C. Prussian Blue Analogue-derived co/fe bimetallic nanoparticles immobilized on S/N-doped carbon sheet as a magnetic heterogeneous catalyst for activating peroxymonosulfate in water. *Chemosphere* **2020**, 244, 125444.
- (267) Yang, S.; Qiu, X.; Jin, P.; Dzakpasu, M.; Wang, X. C.; Zhang, Q.; Yang, L.; Ding, D.; Wang, W.; Wu, K. MOF-templated synthesis of

- CoFe₂O₄ nanocrystals and its coupling with peroxymonosulfate for degradation of bisphenol A. *Chem. Eng. J.* **2018**, *353*, 329–339.
- (268) Ye, J.; Li, C.; Wang, L.; Wang, Y.; Dai, J. Synergistic multiple active species for catalytic self-cleaning membrane degradation of persistent pollutants by activating peroxymonosulfate. *J. Colloid Interface Sci.* **2021**, 587, 202–213.
- (269) Chen, Q.; Liu, Y.; Lu, Y.; Hou, Y.; Zhang, X.; Shi, W.; Huang, Y. Atomically dispersed Fe/Bi dual active sites single-atom nanozymes for cascade catalysis and peroxymonosulfate activation to degrade dyes. *J. Hazard. Mater.* **2022**, 422, 126929.
- (270) Cui, P.; Yang, Q.; Liu, C.; Wang, Y.; Fang, G.; Dionysiou, D. D.; Wu, T.; Zhou, Y.; Ren, J.; Hou, H. An N, S-Anchored Single-Atom Catalyst Derived from Domestic Waste for Environmental Remediation. ACS EST Engg. 2021, 1 (10), 1460–1469.
- (271) Zhou, X.; Ke, M.-K.; Huang, G.-X.; Chen, C.; Chen, W.; Liang, K.; Qu, Y.; Yang, J.; Wang, Y.; Li, F. Identification of Fenton-like active Cu sites by heteroatom modulation of electronic density. *Proc. Nat. Acad. Sci.* **2022**, *119* (8), e2119492119.
- (272) Choong, Z.-Y.; Lin, K.-Y. A.; Lisak, G.; Lim, T.-T.; Oh, W.-D. Multi-heteroatom-doped carbocatalyst as peroxymonosulfate and peroxydisulfate activator for water purification: A critical review. *J. Hazard. Mater.* **2022**, 426, 128077.
- (273) He, D.; Zhu, K.; Huang, J.; Shen, Y.; Lei, L.; He, H.; Chen, W. N, S co-doped magnetic mesoporous carbon nanosheets for activating peroxymonosulfate to rapidly degrade tetracycline: Synergistic effect and mechanism. *J. Hazard. Mater.* **2022**, *424*, 127569.
- (274) Zhu, G.; Zhu, J.; Fu, X.; Liu, Q.; Cao, F.; Li, Y.-n.; Qin, Q.; Jiao, M. Co nanoparticle-embedded N, O-codoped porous carbon nanospheres as an efficient peroxymonosulfate activator: singlet oxygen dominated catalytic degradation of organic pollutants. *Phys. Chem. Chem. Phys.* **2020**, 22 (27), 15340–15353.
- (275) Gao, Y.; Zhu, Y.; Chen, Z.; Hu, C. Nitrogen-coordinated cobalt embedded in a hollow carbon polyhedron for superior catalytic oxidation of organic contaminants with peroxymonosulfate. *ACS EST Engg.* **2021**, *1* (1), 76–85.
- (276) Gao, Y.; Zhu, Y.; Lyu, L.; Zeng, Q.; Xing, X.; Hu, C. Electronic structure modulation of graphitic carbon nitride by oxygen doping for enhanced catalytic degradation of organic pollutants through peroxymonosulfate activation. *Environ. Sci. Technol.* **2018**, 52 (24), 14371–14380.
- (277) Ji, X.; Huang, J.-W.; Liu, W.-J.; Yu, H.-Q. Pyrolysis of Biomass Wastes to N-Doped Biochar-Stabilized Co Nanoparticles for Efficient Pollutant Degradation Via Peroxymonosulfate Activation. *ACS EST Engg.* **2021**, *1* (12), 1715–1724.
- (278) Lin, K.-Y. A.; Zhang, Z.-Y. Degradation of Bisphenol A using peroxymonosulfate activated by one-step prepared sulfur-doped carbon nitride as a metal-free heterogeneous catalyst. *Chem. Eng. J.* **2017**, *313*, 1320–1327.
- (279) Liu, B.; Guo, W.; Wang, H.; Si, Q.; Zhao, Q.; Luo, H.; Ren, N. B-doped graphitic porous biochar with enhanced surface affinity and electron transfer for efficient peroxydisulfate activation. *Chem. Eng. J.* **2020**, *396*, 125119.
- (280) Wang, Y.; Liu, M.; Zhao, X.; Cao, D.; Guo, T.; Yang, B. Insights into heterogeneous catalysis of peroxymonosulfate activation by boron-doped ordered mesoporous carbon. *Carbon* **2018**, *135*, 238–247.
- (281) Zhu, S.; Huang, X.; Yang, X.; Peng, P.; Li, Z.; Jin, C. Enhanced transformation of Cr(VI) by heterocyclic-N within nitrogen-doped biochar: impact of surface modulatory persistent free radicals (PFRs). *Environ. Sci. Technol.* **2020**, *54* (13), 8123–8132.
- (282) Duan, X.; Indrawirawan, S.; Sun, H.; Wang, S. Effects of nitrogen-, boron-, and phosphorus-doping or codoping on metal-free graphene catalysis. *Catal. Today* **2015**, 249, 184–191.
- (283) Li, Y.; Li, S.; Wang, Y.; Wang, J.; Liu, H.; Liu, X.; Wang, L.; Liu, X.; Xue, W.; Ma, N. Electrochemical synthesis of phosphorus-doped graphene quantum dots for free radical scavenging. *Phys. Chem. Chem. Phys.* **2017**, *19* (18), 11631–11638.
- (284) Chen, W.; Gao, W.; Tu, P.; Robert, T.; Ma, Y.; Shan, H.; Gu, X.; Shang, W.; Tao, P.; Song, C. Neighboring Pt atom sites in an ultrathin

- FePt Nanosheet for the efficient and highly CO-tolerant oxygen reduction reaction. *Nano Lett.* **2018**, *18* (9), 5905–5912.
- (285) Chu, C.; Huang, D.; Gupta, S.; Weon, S.; Niu, J.; Stavitski, E.; Muhich, C.; Kim, J.-H. Neighboring Pd single atoms surpass isolated single atoms for selective hydrodehalogenation catalysis. *Nat. Commun.* **2021**, *12*, 5179.
- (286) Xia, C.; Qiu, Y.; Xia, Y.; Zhu, P.; King, G.; Zhang, X.; Wu, Z.; Kim, J. Y. T.; Cullen, D. A.; Zheng, D. General synthesis of single-atom catalysts with high metal loading using graphene quantum dots. *Nat. Chem.* **2021**, *13* (9), 887–894.
- (287) Jia, Q.; Ramaswamy, N.; Hafiz, H.; Tylus, U.; Strickland, K.; Wu, G.; Barbiellini, B.; Bansil, A.; Holby, E. F.; Zelenay, P. Experimental observation of redox-induced Fe—N switching behavior as a determinant role for oxygen reduction activity. *ACS Nano* **2015**, 9 (12), 12496–12505.
- (288) Li, J.; Ghoshal, S.; Liang, W.; Sougrati, M.-T.; Jaouen, F.; Halevi, B.; McKinney, S.; McCool, G.; Ma, C.; Yuan, X. Structural and mechanistic basis for the high activity of Fe-N-C catalysts toward oxygen reduction. *Ener. Environ. Sci.* **2016**, *9* (7), 2418–2432.
- (289) Li, X.; Zeng, Y.; Tung, C.-W.; Lu, Y.-R.; Baskaran, S.; Hung, S.-F.; Wang, S.; Xu, C.-Q.; Wang, J.; Chan, T.-S. J. A. C. Unveiling the in situ generation of a monovalent Fe (I) site in the single-Fe-atom catalyst for electrochemical ${\rm CO_2}$ reduction. ACS Catal. 2021, 11 (12), 7292–7301.
- (290) Xiao, M.; Zhu, J.; Ma, L.; Jin, Z.; Ge, J.; Deng, X.; Hou, Y.; He, Q.; Li, J.; Jia, Q. J. A. C. Microporous framework induced synthesis of single-atom dispersed Fe-NC acidic ORR catalyst and its in situ reduced Fe-N₄ active site identification revealed by X-ray absorption spectroscopy. ACS Catal. **2018**, 8 (4), 2824–2832.
- (291) Zeng, Y.; Li, X.; Wang, J.; Sougrati, M. T.; Huang, Y.; Zhang, T.; Liu, B. In situ/operando Mössbauer spectroscopy for probing heterogeneous catalysis. *Chem. Catal.* **2021**, *1* (6), 1215–1233.
- (292) Fang, L.; Seifert, S.; Winans, R. E.; Li, T. Operando XAS/SAXS: Guiding Design of Single-Atom and Subnanocluster Catalysts. *Small Methods* **2021**, *5* (5), 2001194.
- (293) Rodrigues, T. Deriving intuition in catalyst design with machine learning. *Chem.* **2022**, *8* (1), 15–17.
- (294) Zhu, C.; Nie, Y.; Zhao, S.; Fan, Z.; Liu, F.; Li, A. Constructing Surface Micro-Electric Fields on Hollow Single-Atom Cobalt Catalyst for Ultrafast and Anti-Interference Advanced Oxidation. *Appl. Catal. B Environ.* **2022**, 305, 121057.
- (295) Zheng, W.; You, S.; Yao, Y.; Jin, L.; Liu, Y. Development of Atomic Hydrogen-Mediated Electrocatalytic Filtration System for Peroxymonosulfate Activation Towards Ultrafast Degradation of Emerging Organic Contaminants. *Appl. Catal. B Environ.* **2021**, 298, 120593.
- (296) Pan, M.; Wang, J.; Gao, G.; Chew, J. W. Incorporation of single cobalt active sites onto N-doped graphene for superior conductive membranes in electrochemical filtration. *J. Membr. Sci.* **2020**, *602*, 117966.
- (297) Sun, M.; Wang, X.; Winter, L. R.; Zhao, Y.; Ma, W.; Hedtke, T.; Kim, J.-H.; Elimelech, M. Electrified Membranes for Water Treatment Applications. *ACS EST Engg.* **2021**, *1* (4), 725–752.
- (298) Lin, H.; Wu, J.; Zhang, H. Degradation of clofibric acid in aqueous solution by an EC/Fe³⁺/PMS process. *Chem. Eng. J.* **2014**, 244, 514–521.
- (299) Zhang, S.; Hedtke, T.; Zhou, X.; Elimelech, M.; Kim, J.-H. Environmental Applications of Engineered Materials with Nanoconfinement. ACS EST Engg. 2021, 1 (4), 706–724.